The Swiss - Norwegian Beam Lines at ESRF

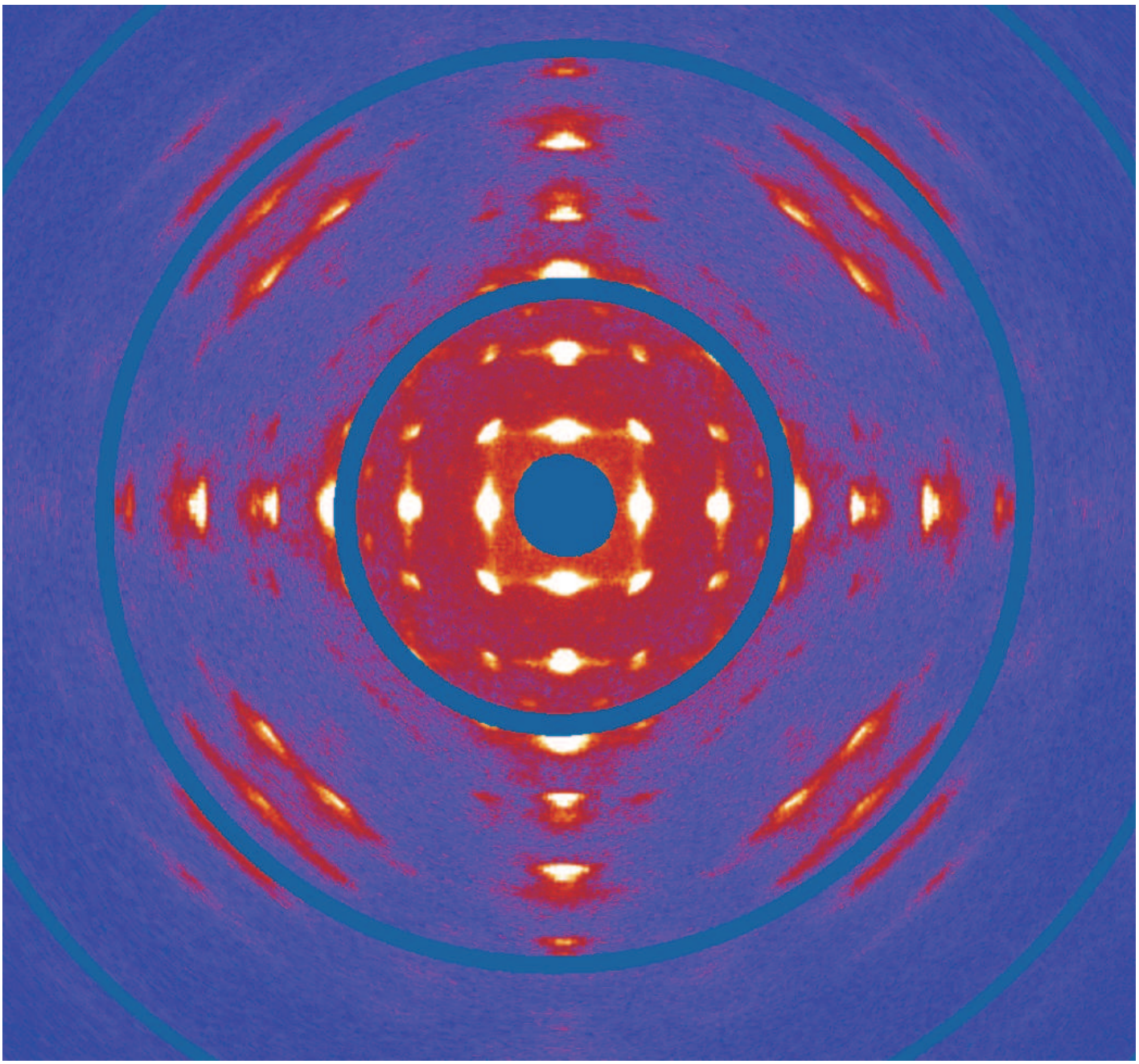

15/16

ACTIVITY REPORT

CONTENTS

SCIENTIFIC HIGHLIGHTS

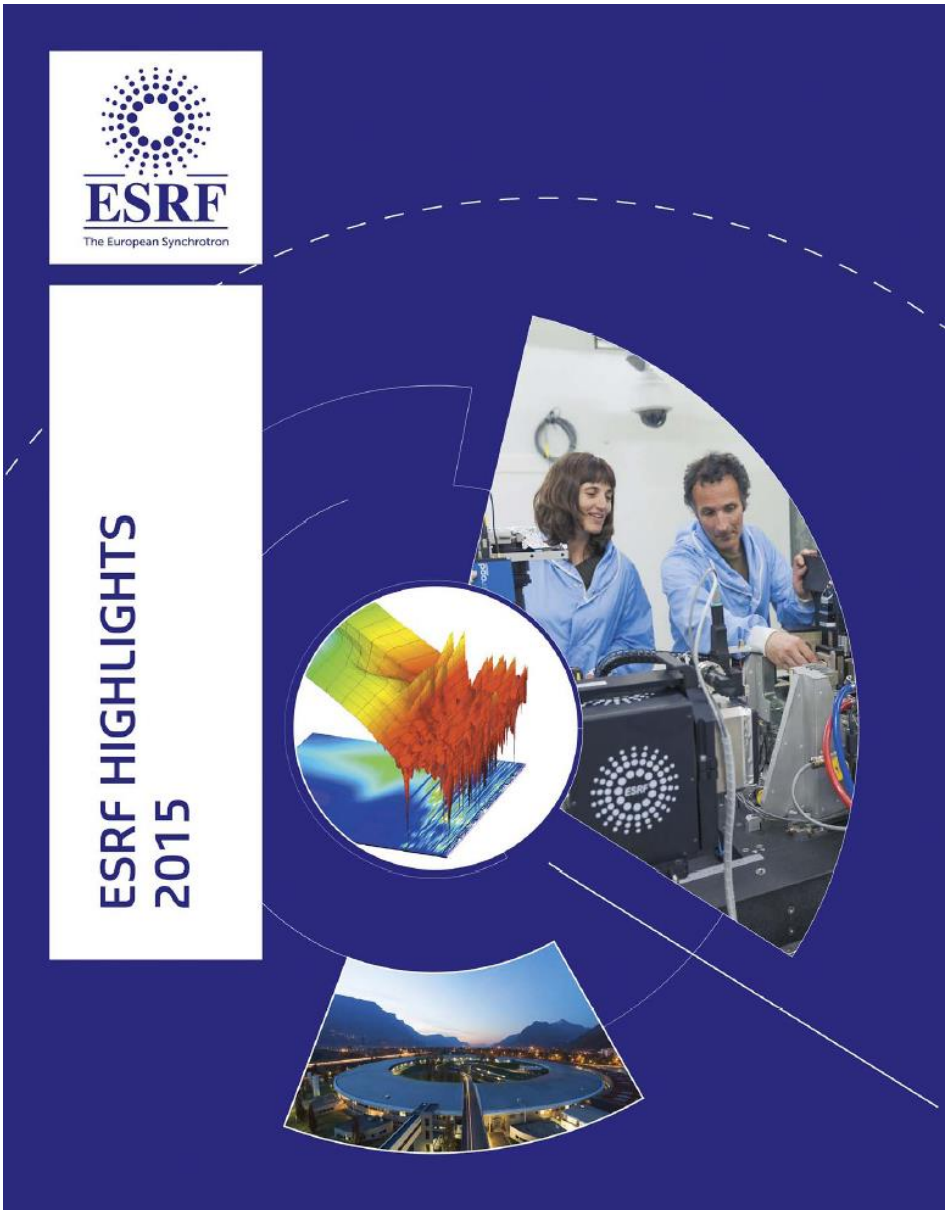

STRUCTURE OF MATERIALS

MIXED-ANION METAL BORANES FOR SOLID STATE Na AND Li ELECTROLYTES

Na-based materials are becoming competitive alternatives to Li-ion batteries. For all-solid battery systems, electrode and electrolyte materials need to be developed and tested. Simple packed compounds have been discovered based on the tetrahydroborate $[BH_4]^-$ (borohydride) and the dodecahydroborate $[B_{12}H_{12}]^{2-}$ (*closo*borane) anions with very high conductivities for Li^+ and Na^+ cations comparable to NASICON-type materials, sulphide-glasses and rivalling even superionic β-alumina.

Much battery research is currently oriented towards the development of all-solid state concepts, where the liquid electrolyte, usually based on an organic solvent that dissolves the mobile species, *e.g.* Li^+ in Li-ion batteries, is replaced by a polymer or solid electrolyte. The aim is to avoid the safety issues arising with conventional, flammable liquid electrolytes. While such modifications eliminate the risk of dendritic growth or failure due to bad electrochemical and thermal stability of the cell, they pose a challenge with respect to the mobility of charge carriers, commonly orders of magnitude lower in the solid state than in the liquid.

Li-ion batteries are currently considered the benchmark technology for mobile applications. However, tremendous efforts are being invested on a global scale to take both mobile and stationary applications beyond lithium. These targets include large-scale implementations such as grid energy storage, where low power density can be compensated for by quantity or size. Hence, Na-based materials could become competitive alternatives. For all-solid battery systems, electrode and electrolyte materials need to be developed and tested.

This study deals with the solid-state electrolyte. Electrochemically stable materials with a large operating voltage window and a high conductivity at room temperature (RT) are required, potentially allowing a battery-design that employs metallic Na as anode-material, thus providing high capacity. Ionic conduction in a solid-state electrolyte is promoted by vacancy-driven mechanisms as well as structural dynamics. In particular, the *bcc* anion lattice has been found to favour ionic mobility. Novel materials that contain poly-anions $[AB_y]^{n-}$, where the structure is rationalised as a salt, are also promising. In such compounds the energy barrier for ionic conduction is lowered due to the rotational mobility of the poly-anion, which acts as a "paddle wheel" on the mobile ionic species, loosely bound in the host framework.

A number of solid state boranes are available to materials scientists exploring the conductive properties of complex hydrides. The present

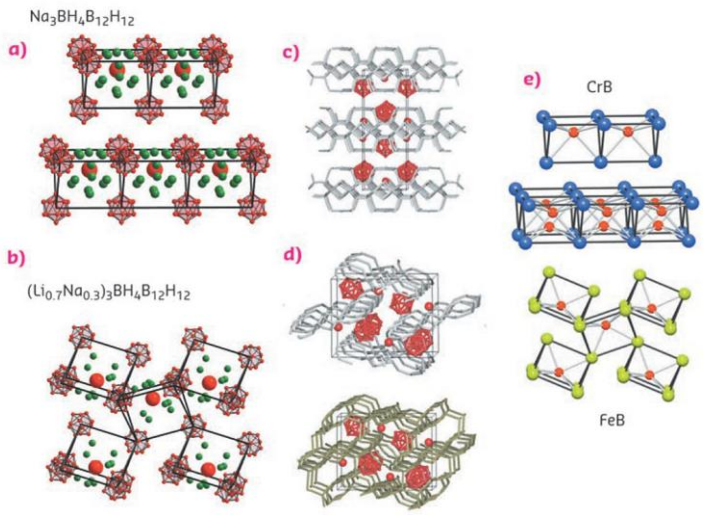

Fig. 42: (a) Crystal structure of $Na_3BH_4B_{12}H_{12}$ and (b) $(Li_{0.7}Na_{0.3})_3BH_4B_{12}H_{12}$; mobile species ($Li^+$,$Na^+$) in green, boron as red spheres, $[B_{12}H_{12}]^{2-}$ as molecule. (c) and (d) Conduction pathways for Na (grey) and Li (brown). (e) Comparison with the prototypical relationship between CrB and FeB; boron in red.

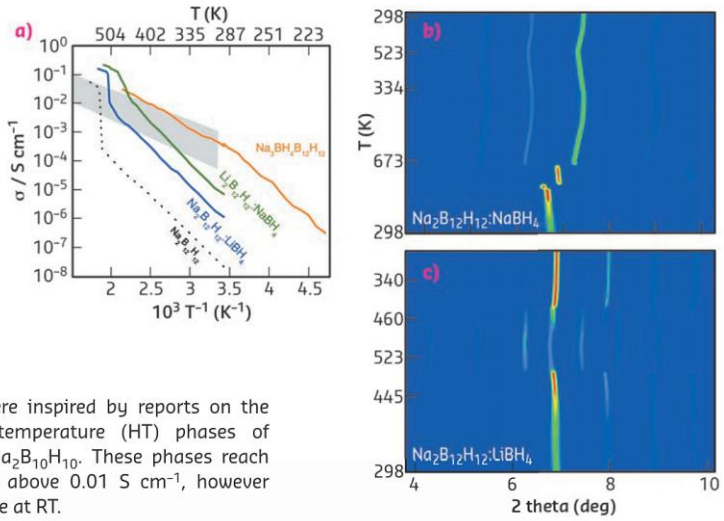

Fig. 43: (a) Ionic conductivities obtained from impedance spectroscopy. Typical NASICON and β-alumina materials in the shaded field. (b) *In situ* temperature-dependent diffraction data for the reaction forming $Na_3BH_4B_{12}H_{12}$ and (c) $(Li_{0.7}Na_{0.3})_3BH_4B_{12}H_{12}$.

investigations were inspired by reports on the superionic high-temperature (HT) phases of $Na_2B_{12}H_{12}$ and $Na_2B_{10}H_{10}$. These phases reach HT-conductivities above 0.01 S cm^{-1}, however they are not stable at RT.

Here, we explore anion-mixing of the tetrahydroborate $[BH_4]^-$ (borohydride) and the dodecahydroborate $[B_{12}H_{12}]^{2-}$ (*closo*borane) anions, attempting to build stable anion-sublattices of high crystal symmetry using the larger *closo*borane, while implementing additional rotational mobility with the borohydride anion. We discovered simple packed compounds and provide a roadmap based on crystal chemistry arguments to explore the phase diagram $Na_3BH_4B_{12}H_{12}$ – $Li_3BH_4B_{12}H_{12}$ in a search for further anion-mixed single- and double-cation conductors.

$Na_3BH_4B_{12}H_{12}$ and $(Li_{0.7}Na_{0.3})_3BH_4B_{12}H_{12}$ show very high conductivities of close to, and above, 10^{-1} S cm^{-1} at 500 K (Figure 42). To monitor HT reactions forming the solid electrolytes, we chose to work with the 2D Dectris Pilatus detector at **BM01A**, which allows very high counting statistics to be acquired at a fast rate (Figure 43). The crystal structures of the novel materials (Figure 42) provide evidence of localisation of the mobile species, Na^+ and Na^+/Li^+, respectively, in the structural fragments containing the borohydride anion, supporting the concept of anion-engineering, one of the initial aims of this project.

Topologically, a 1-dimensional conduction path is accessible to the Na-species in $(Li_{0.7}Na_{0.3})_3BH_4B_{12}H_{12}$, while a 2-dimensional path is available to Li (Figure 42), theoretically both species can conduct. However, the material is subject to a reversal chemical reaction upon cooling, and dissociates to its precursors. Upon heating, it again forms the superionic phase at 500 K (Figure 43).

$Na_3BH_4B_{12}H_{12}$, on the other hand, is formed by a reaction between $Na_2B_{12}H_{12}$ and $NaBH_4$ at 673 K, and is stable at RT. The 2D conduction pathways allow this phase to reach RT-conductivity values close to 10^{-2} S cm^{-1}, comparable to NASICON-type materials, sulphide-glasses and rivalling even superionic β-alumina. Next to the electrochemical stability of $Na_3BH_4B_{12}H_{12}$ (up to 10 V) and the favourable mechanical properties due to the material softness, the high RT-conductivity implies the potential use of Na-metal as anode. Furthermore, the reducing nature of the material minimises the risk of surface reactions on the electrode.

Our structural analyses have revealed a most striking similarity to the relationship between different stacking variants of metal-borides, which points towards the existence of further electrolytes in the $Na_3BH_4B_{12}H_{12}$ – $Li_3BH_4B_{12}H_{12}$ diagram, simply related by polytypism.

PRINCIPAL PUBLICATION AND AUTHORS

Superionic conduction of sodium and lithium in anion-mixed hydroborates $Na_3BH_4B_{12}H_{12}$ and $(Li_{0.7}Na_{0.3})_3BH_4B_{12}H_{12}$, Y. Sadikin, M. Brighi, P. Schouwink and R. Černý, *Adv. Energ. Mater.* 1501016 (2015); doi: 10.1002/aenm.201501016.

Laboratory of Crystallography, Department of Quantum Matter Physics, University of Geneva (Switzerland)

STRUCTURE OF MATERIALS

STRUCTURE AND PROPERTIES OF COMPLEX HYDRIDE PEROVSKITE MATERIALS

Borohydride perovskites pave the way to functional design in complex hydride materials for energy-applications. A novel mechanism is suggested for symmetry-design in perovskites, arising from the hydridic nature of hydrogen and inverting the temperature-dependency of lattice instabilities.

Perovskite materials are ubiquitous in materials science because of their distinct adjustability of physical properties and the readiness to incorporate most chemical elements from the periodic table. Slight alterations of the crystal structure can induce dramatic changes in the physical properties. Widely known as reducing agents in organic chemistry, the high hydrogen content per unit mass/volume and the rich structural dynamics of metal borohydrides have triggered vast investigations on their energy-related implementation as materials for solid-state hydrogen storage and all-solid batteries. Initially this was driven by the potential to develop $LiBH_4$ into a storage medium for on-board automobile applications. The motivation behind metal borohydrides in the materials science community hence directly targets a prime issue of modern consumer societies.

Due to the hydridic nature of hydrogen in the BH_4-molecule, borohydrides are somewhat an outsider, chemically speaking. The covalently bound hydrogen in molecular chemistry commonly carries a positive formal charge (protic hydrogen).

Despite the application-oriented search for novel complex hydrides, the rational structure-property design of metal borohydrides is still in its infancy. The principal objective of this study was to provide an extensive characterisation of a host material capable of meeting the requirements of genuine functional design, in order to take borohydrides beyond hydrogen storage applications in the future. Ideally, such a host material is of reduced complexity and superior stability.

Motivated by our previous discovery of a double-cation borohydride $KMn(BH_4)_3$ crystallising in the perovskite lattice, this structure type was systematically explored leading to the discovery of over 45 different materials whose formability criteria were evaluated based on the commonly used Goldschmidt tolerance factor (Figure 44).

We began to study this field on powder samples prepared by mechanochemistry using the Dectris Pilatus M2 detector at **BM01A**, systematically heating the sample to its decomposition (detection of thermal stability). With the resulting materials, we have managed to produce metal borohydrides with unforeseen

a)

	Mg	Mn	YLi	MgCa	Ca	Sr	Eu	Pb	RbY	CsY	CsGd
Na	0.819	0.789	0.789	0.781	0.747	0.707	0.709				
K	0.900	0.867	0.867	0.855	0.820	0.776	0.779	0.774			
Rb	0.917	0.883	0.884	0.875	0.836	0.797	0.793	0.795	0.777	0.759	
Cs	0.956	0.921	0.921	0.912	0.872	0.825	0.827	0.822	0.810	0.792	0.787
NH_4	0.947	0.846	0.846	0.837	0.800	0.757	0.760				

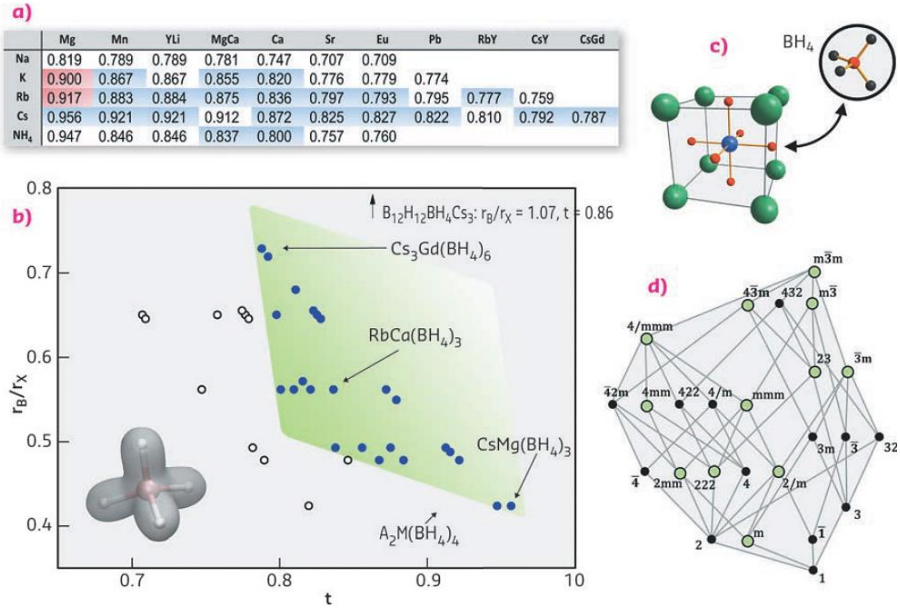

Fig. 44: (a-b) Formability field (green) of borohydride perovskites based on octahedral vs. tolerance factor *t* (listed in table (a). The $AM(BH_4)_3$ structure is shown in (c). (d) Sub-groups of the cubic aristotype, green circles correspond to crystal symmetries of discovered borohydrides.

physical properties such as photoluminescence, magnetic refrigeration, semiconductivity, and proton-hydride interactions between cations NH_4^+ and anions BH_4^- which facilitate H_2-formation. Simple concepts such as the tolerance factor and ionic substitution were applied in order to obtain a desired property, following the established approaches for metal-oxide perovskites.

An unexpected structural trend was revealed for metal-borohydride perovskites. For perovskites in general, both the rotation (tilt) of MO_6 octahedra and atomic displacements tend to vanish upon heating due to an increase in crystal symmetry, likewise for polar physical properties, such as an electric dipole moment. But for $AM(BH_4)_3$ (A: alkali metal, M: bivalent metal), we often find this trend to be reversed, hence stabilising low crystal symmetry at high temperature, and providing the structural requirements for polar properties. Our working hypothesis assigns the origin of this behaviour to interactions between molecular B-H vibrations and lattice vibrations and hence proposes a novel mechanism useful for tailoring perovskite symmetries [1]. For instance, a prominent lattice instability (*R*-point) of symmetry *Pnma* is activated upon heating $KCa(BH_4)_3$ into the HT-phase (Figure 45). A discrete step in the bandwidth of the Raman B-H stretching signature concurs with the structural transition, suggesting that internal modes of the BH_4 molecule and lattice modes stabilising the crystal symmetry communicate with each other.

Theoretical solid state calculations provided further insight into the transformation mechanism, pointing towards the crucial role of close homopolar repulsive di-hydrogen for the structural behaviour of $AM(BH_4)_3$ (Figure 45). As well as providing a stable host for functional design, the borohydride perovskite hence incorporates weak interactions, which define structure and packing in molecular and supramolecular chemistry, into a structural behaviour otherwise controlled by lattice vibrations. Meanwhile, the role of these interactions in $AM(BH_4)_3$ has been verified by quasielastic neutron scattering studies of BH_4 reorientations [2] and single crystal X-ray diffraction performed at **BM01A** on the first double-cation metal-borohydride single crystal [3].

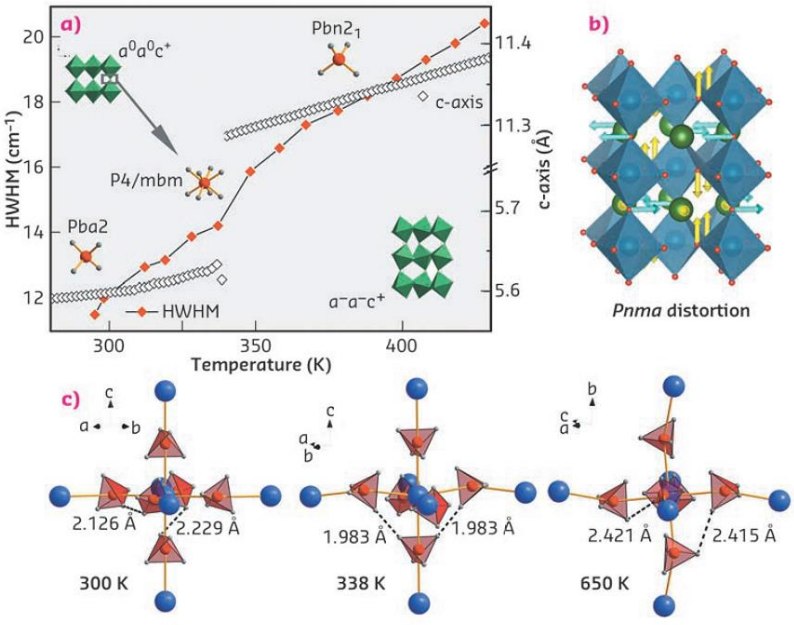

Fig. 45: (a) Changes in structure during the high-temperature phase transition of $KCa(BH_4)_3$, followed by *in situ* powder diffraction and Raman spectroscopy; (b) The corresponding apolar parent distortion; (c) relevant short H···H contacts within the $Ca(BH_4)_6$-octahedron.

PRINCIPAL PUBLICATION AND AUTHORS

P. Schouwink (a), M.B. Ley (b), A. Tissot (c), H. Hagemann (c), T.R. Jensen (b), L. Smrčok (d) and R. Černý (a), *Nature Comm.* **5**, 5706 (2014).
(a) Laboratory of Crystallography, Department of Quantum Matter Physics, University of Geneva (Switzerland)
(b) Interdisciplinary Nanoscience Center (iNANO), Department of Chemistry, University of Aarhus (Denmark)
(c) Department of Physical Chemistry, University of Geneva (Switzerland)
(d) Institute of Inorganic Chemistry, Slovak Academy of Sciences, Bratislava, (Slovak Republic)

REFERENCES

[1] J.M. Rondinelli and C.J. Fennie, in *Adv. Mater.* **24**, 1961-1968 (2012).
[2] P. Schouwink *et al.*, in *J. Phys. Condens. Matt.*, **27**, 265403 (2015).
[3] P. Schouwink *et al.*, in *CrystEngComm*, **17**, 2682-2689 (2015).


ESRF
The European Synchrotron
ESRF HIGHLIGHTS
2016

ELECTRONIC STRUCTURE, MAGNETISM AND DYNAMICS

SPIRAL SPIN-LIQUID AND THE EMERGENCE OF A VORTEX-LIKE STATE IN $MnSc_2S_4$

Spiral spin-liquid is a short-range correlated state where spins fluctuate collectively as spirals in real space. Such a correlation is highly unusual: in conventional paramagnets, spins fluctuate in a completely random fashion. We present direct experimental evidence for the existence of the spiral spin-liquid state in A-site spinels, reveal the multi-step ordering of the spiral spin liquid and discover a vortex-like triple-*q* phase on application of a magnetic field.

The A-site spinel $MnSc_2S_4$ is a promising candidate to realise the spiral spin-liquid state [1,2]. In $MnSc_2S_4$, Mn^{2+} (S = 5/2) ions occupy the A-sites and constitute a diamond lattice as is shown in **Figure 27a**. The bi-partite character of the diamond lattice allows the definition of the J_1-J_2 model, with the ferromagnetic J_1 and the antiferromagnetic J_2 couplings. In the weak frustration regime of $J_2/J_1 < 0.125$, the spin correlations are similar to that of conventional paramagnets. However, in the strong frustration regime of $J_2/J_1 > 0.125$, the propagation vector will form a continuous surface in the reciprocal space, shown in **Figure 27b**. Since each q-vector on this surface represents a spiral state under the mean-field theory, such a continuous surface is named the 'spiral surface'. Previous experiments using a powder sample of $MnSc_2S_4$ have revealed a long-range order transition at T_N = 2.3 K and suggested the existence of the spiral surface at $T > T_N$ [3]. However, direct proof of the spiral surface was missing, which requires single crystal samples.

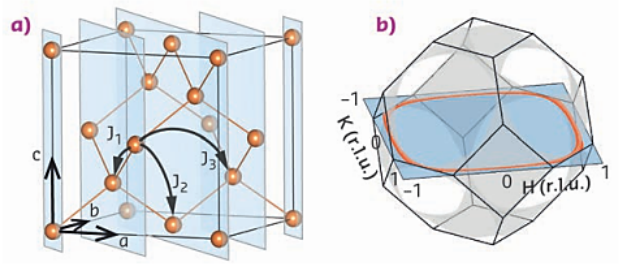

Fig. 27: a) Mn^{2+} ions in $MnSc_2S_4$ constitute a diamond lattice. b) The predicted spiral surface (grey) in $MnSc_2S_4$ with the frustration ratio J_2/J_1 = 0.85.

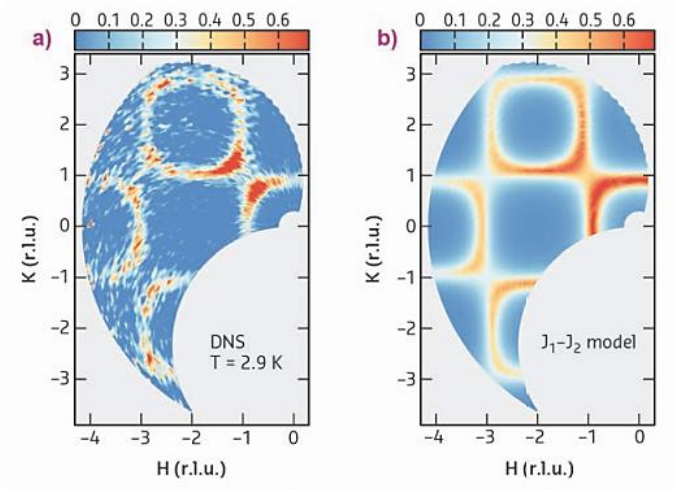

Fig. 28: a) Diffuse neutron scattering results measured on DNS at 2.9 K. The 50 K data has been subtracted as the background. b) Monte Carlo simulation results using the J_1-J_2 model with a frustration ratio of J_2/J_1 = 0.85.

Recently we succeeded in growing single crystals of $MnSc_2S_4$ using the chemical transport technique. To check the quality, we performed single-crystal synchrotron diffraction experiments at beamline BM01 (Swiss-Norwegian CRG beamline). Altogether 2738 Bragg reflections were collected at room temperature, our refinement of the spinel structure did not detect any Mn-Sc anti-site disorder and confirmed the good quality of our single crystals.

To study the short-range correlations in $MnSc_2S_4$, we performed polarised neutron diffuse scattering experiments on DNS at MLZ. **Figure 28a** presents the results measured at T = 2.9 K. A squared ring feature near the Brillouin zone boundary can be clearly resolved, which is consistent with the existence of the spiral surface. Considering that the spiral surface extends towards the zone boundary with increasing frustration ratio J_2/J_1, it is clear that the frustration should be strong in $MnSc_2S_4$.

To fix the frustration ratio J_2/J_1 in $MnSc_2S_4$, we performed classical Monte Carlo simulations using the ALPS package [4]. As shown in **Figure 28b**, the simulation results with J_2/J_1 = 0.85 can reproduce the observed squared ring feature very well. Such a high ratio of J_2/J_1 puts $MnSc_2S_4$ deep in the spiral spin-liquid phase [1] and thus the observed ring feature is direct evidence of the spiral surface.

Besides the spiral spin-liquid state, we also investigated the long-range ordered state at $T < T_N$ performing single crystal neutron diffraction on TriCS at SINQ of PSI and spherical neutron polarimetry on TASP with MuPAD at SINQ and IN22 with CryoPAD at ILL. Our experiments revealed multi-step transitions: at 2.2 K, the system first enters a sinusoidally modulated collinear phase with q = [0.75 0.75 0]; at 1.64 K, it then enters a transitional incommensurate phase with q = [0.75±0.02 0.75±0.02 0]; and finally, at 1.46 K, the system enters a helical phase with q back to the [0.75 0.75 0] position. Such a multi-step transition is direct evidence of the importance of perturbations from the third-neighbour coupling J_3 and the dipolar interactions **[2]**.

Under a magnetic field along the [001] direction, a triple q phase with $\Sigma_i q_i = 0$ is observed through the analysis of the domain population. Although neutron diffraction is not sensitive to the phase factor, candidate structures all exhibit a winding feature for the spin components in the [111] plane. Therefore the observed triple-q structure is in fact a vortex lattice. We note that the q-combination rule of the triple-q phase is very similar to that of the skyrmion lattice **[5]**.

PRINCIPAL PUBLICATION AND AUTHORS

Spiral spin-liquid and the emergence of a vortex-like state in $MnSc_2S_4$, S. Gao (a,b), O. Zaharko (a), V. Tsurkan (c,d), Y. Su (e), J.S. White (a), G.S. Tucker (a,f), B. Roessli (a), F. Bourdarot (g), R. Sibille (a,h), D. Chernyshov (i), T. Fennell (a), A. Loidl (c) and C. Rüegg (a,b), *Nature Physics* (2016); doi: 10.1038/nphys3914.

(a) Laboratory for Neutron Scattering and Imaging, Paul Scherrer Institut, Villigen PSI (Switzerland)
(b) Department of Quantum Matter Physics, University of Geneva (Switzerland)
(c) Experimental Physics V, University of Augsburg (Germany)
(d) Institute of Applied Physics, Academy of Sciences of Moldova, Chisinau (Republic of Moldova)
(e) Jülich Center for Neutron Science JCNS-MLZ, Forshungszentrum Jülich GmbH, Outstation at MLZ, Garching (Germany)
(f) Laboratory for Quantum Magnetism, École Polytechnique Fédérale de Lausanne (Switzerland)
(g) CEA et Université Grenoble Alpes, INAC-MEM-MDN, Grenoble (France)
(h) Laboratory for Scientific Developments and Novel Materials, Paul Scherrer Institut, Villigen PSI (Switzerland)
(i) Swiss-Norwegian Beamlines at the ESRF, Grenoble (France)

REFERENCES

[1] D. Bergman *et al.*, Nat. Phys. 3, 487 (2007)
[2] S. B. Lee *et al.*, Phys. Rev. B 78, 144417 (2008)
[3] A. Krimmel *et al.*, Phys. Rev. B 73, 014413 (2006)
[4] B. Bauer *et al.*, *J. Stats. Mech.* **2011**, P05011 (2011)
[5] S. Mühlbauer *et al.*, *Sci.* **323**, 915 (2009).

NEW TYPE OF CHARGE-ORDERING TRANSITION IN THE NOVEL IRON OXIDE Fe_4O_5

Synthesis of new classes of compounds can lead to discoveries of novel physical phenomena as well as innovative applications. Fe_4O_5 is the first member of a very recently discovered family of iron oxides that can be synthesised only under high-pressure conditions. A multi-technique study of Fe_4O_5 reveals that it undergoes a unique charge-ordering transition below 150 K that involves competing dimeric and trimeric ordering within the chains of Fe ions. This electronic transition drives an intricate incommensurate distortion in its crystal structure.

At ambient pressure, only three iron oxide polymophs were known, FeO, Fe_3O_4, and Fe_2O_3. Recently, several new iron oxide polymorphs with hitherto unknown stoichiometries have been discovered under high pressure conditions **[1,2]**. Among them, Fe_4O_5 looks particularly exciting as it can be readily quenched at ambient pressure **[1]**. We have performed a series of low-temperature studies on a recently-discovered high-pressure polymorph of iron oxide, Fe_4O_5 **[1]** and discovered a new type of charge-ordering transition involving the formation of competing dimeric and trimeric ordering within the chains of Fe ions, as revealed by X-ray diffraction studies at beamline **BM01**, SNBL. These findings were supported in neutron diffraction experiments and in measurements of magnetic and transport properties. To date, such exotic transitions have never been observed, and, hence, it brings new perspectives on charge-ordered states and transitions.

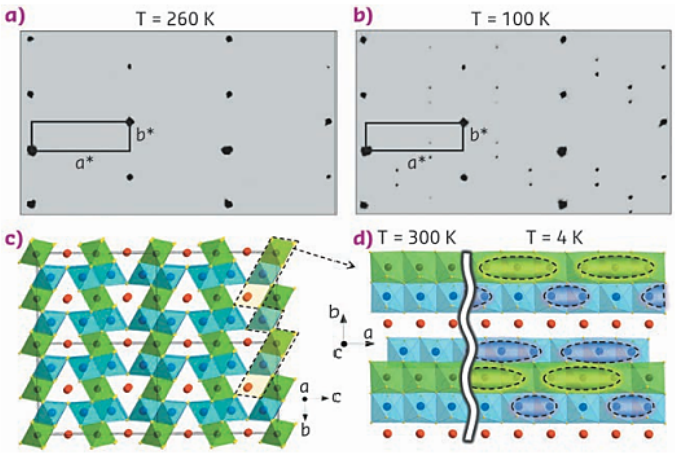

Fig. 129: (a, b) Examples of reciprocal lattices of X-ray diffraction intensities of Fe_4O_5 at 260 K and 100 K (c) Crystal structure projected down the *a*-axis at room temperature. d) Crystal structure of Fe_4O_5 projected along the *c*-axis at room and low temperatures.

At ambient conditions, Fe_4O_5 crystallises in a $CaFe_3O_5$-type structure featuring linear chains of octahedrally-coordinated iron ions and linear chains of FeO_6 trigonal prisms along the *a*-axis (**Figure 129a,c**). This compound contains equal amounts of Fe^{2+} and Fe^{3+} ions, and like another mixed-valent iron oxide, magnetite (Fe_3O_4), it is a good electrical conductor owing to a charge transfer between Fe^{2+} (charges) and Fe^{3+} (vacancies). Magnetite is known to undergo a charge-ordering phase transition below 125 K, which is accompanied by a jump in electrical resistivity **[3]**. This transition in magnetite had been discovered by Verwey in 1939 **[3]**, but only recently by means of single-crystal X-ray diffraction, the charge-ordering pattern in its low-temperature phase has finally been uncovered to involve 'three-site-distortions', called 'trimerons' **[4]**. Analysis of the bond valence sums in the lattice of Fe_4O_5 indicated the mixed valence states of iron at the octahedrally-coordinated sites (**Figure 129c**), and, hence, one could expect that Fe_4O_5 also undergoes some charge ordering at relatively low temperatures.

The high-quality single crystal X-ray diffraction patterns of Fe_4O_5 collected at beamline **BM01** demonstrated the appearance of superlattice reflections upon cooling below 150 K (**Figure 129a,b**). Analysis of these patterns revealed that the low-temperature structure is incommensurately modulated and contains the Fe dimers and trimers within the chains of the octahedrally-coordinated iron (**Figure 129d**). A constant Fe-Fe distance of 2.861 Å (at 4 K) in the trigonal chains of ferrous iron enabled the dramatic shortening of some interoctahedra distances (marked by elongated ellipsoids in **Figure 129d**) to be highlighted. Each chain of

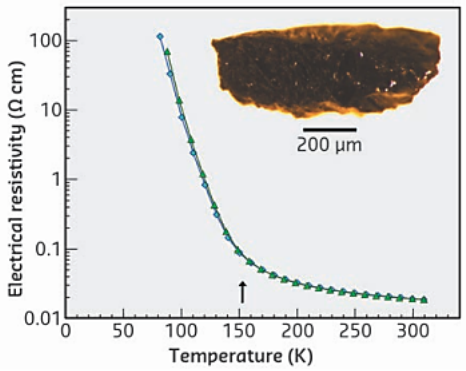

Fig. 130: Temperature dependencies of electrical resistivity of Fe_4O_5 in 0 and 12 T magnetic fields (blue and green curves, respectively). These curves exhibit a bend at 150 K (marked by the arrow), indicating a 'metal-insulator'-type transition. A photograph of the Fe_4O_5 sample is included.

MATTER AT EXTREMES

the octahedral cations contains either dimers composed of Fe^{2+}–Fe^{3+} pairs with one shared electron, or trimers composed of one Fe^{2+} and two Fe^{3+} ions, similar to the trimerons in Fe_3O_4 **[4]** (**Figure 129d**). This unusual charge-ordering transition in Fe_4O_5 is concurrent with a significant increase in electrical resistivity (**Figure 130**), and therefore, it may be classified as a "metal-insulator"-type transition. The magnetic susceptibility measurements and neutron diffraction establish the formation of a collinear antiferromagnetic order above room temperature and a spin canting at 85 K that gives rise to spontaneous magnetisation.

PRINCIPAL PUBLICATION AND AUTHORS

Charge ordering transition in iron oxide Fe_4O_5 involving competing dimer and trimer formation, S.V. Ovsyannikov (a), M. Bykov (a,b), E. Bykova (a,b), D.P. Kozlenko (c), A.A. Tsirlin (d,e), A.E. Karkin (f), V.V. Shchennikov (f,g), S.E. Kichanov (c), H. Gou (a,h), A.M. Abakumov (i,j), R. Egoavil (i), J. Verbeeck (i), C. McCammon (a), V. Dyadkin (k), D. Chernyshov (k), S. van Smaalen (b) and L.S. Dubrovinsky (a), *Nature Chemistry* **8**, 501-508 (2016); doi:10.1038/nchem.2478.

(a) Bayerisches Geoinstitut, Universität Bayreuth (Germany)
(b) Laboratory of Crystallography, Universität Bayreuth (Germany)
(c) Frank Laboratory of Neutron Physics, JINR, Dubna (Russia)
(d) National Institute of Chemical Physics and Biophysics, Tallinn (Estonia)
(e) Institute of Physics, University of Augsburg (Germany)
(f) Institute of Metal Physics, Russian Academy of Sciences, Yekaterinburg (Russia)
(g) Institute for Solid State Chemistry, Russian Academy of Sciences, Yekaterinburg (Russia)
(h) Key Laboratory of Metastable Materials Science and Technology, Yanshan University, Qinhuangdao (China)
(i) Electron Microscopy for Materials Research (EMAT), University of Antwerp (Belgium)
(j) Department of Chemistry, Moscow State University (Russia)
(k) Swiss–Norwegian Beamlines at the ESRF, Grenoble (France)

REFERENCES

[1] B. Lavina, *et al. Proc Nat. Acad. Sci. US* **108**, 17281 (2011).
[2] E. Bykova, *et al.*, *Nature Commun.* **7**, 10661 (2016).
[3] E.J.W. Verwey, *Nature* **144**, 327 (1939).
[4] M.S. Senn *et al.*, *Nature* **481**, 173 (2012).

Capturing metal-support interactions *in situ* during the reduction of a Re promoted Co/γ-Al_2O_3 catalyst

N. E. Tsakoumis,*[a] R. E. Johnsen, [b] W. van Beek, [c] M. Rønning, [a] E. Rytter, [a,d] and A. Holmen [a]

[a]*Department of Chemical Engineering, Norwegian University of Science and Technology (NTNU), NO-7491 Trondheim, Norway.*
[b]*Department of Energy Conversion and Storage, Technical University of Denmark, DK-4000 Roskilde, Denmark.*
[c]*Swiss–Norwegian Beamlines at ESRF, BP 220, Grenoble 38043, France,*
[d]*SINTEF Materials and Chemistry, NO-7465 Trondheim, Norway*

Catalyst activation is a critical step in the start-up procedure for most industrial heterogeneously catalysed processes. Commonly a solid precursor is subjected to conditions that allow its transformation to the catalytically active component. In many catalytic applications, the metallic surface of nanoparticles (NPs) is the active phase and therefore reduction of supported metal oxide precursors precedes. The reduction process is affected by various parameters such as the nature of precursor, the size of the nanoparticles, the reactivity of the support and the reducing atmosphere. Execution of catalyst activation has an impact on the final catalyst structure, involving risks of sintering or a low final degree of reduction [1]. Often catalyst activity and selectivity are related to the reduction extend and the NP size [2]. Consequently, deep control through understanding of phase evolutions during activation protocols is important for the optimization of catalyst performance. In the last decades, *in situ* investigations have boosted catalysis research and allowed the deconvolution of complex phenomena like catalyst activation [3].

Cobalt NPs supported on high surface area porous materials such as γ-Al_2O_3, are used in various industrial processes like Fischer–Tropsch synthesis (FTS) [2] and the hydro-desulfurization reaction [4]. Commonly the active $Co^{(0)}$ phase is formed by H_2 reduction of the Co_3O_4 spinel precursor produced after drying and calcination of the impregnated source. Reduction of promoted and un-promoted γ-Al_2O_3 supported Co_3O_4 NPs has been studied in detail. From the majority of the reports, it is evident that the reduction is a two-step process that reaches polycrystalline metallic Co through a CoO intermediate. The use of dopants like Re promotes the reduction process most likely through H_2 spill-over effects [5].

Although most of the reports agree on the steps of the reduction procedure, formation of mixed compounds of Co with the γ-Al_2O_3 support during reduction has been debated. The mixed phase, due to its amorphous nature, low concentrations and possible chemical similarities with divalent Co species present in other Co oxides, is difficult to be probed. Commonly the high temperature (> 600 ^oC) region of temperature programmed reduction (TPR) profiles is linked to Co species that are difficult to be reduced as a result of strong interaction with the support [6]. The Co-support interaction has been indirectly detected for catalysts calcined at high temperatures (> 500 ^oC) by the lattice expansion of Al_2O_3 as observed by *ex situ* XRPD performed after calcination [6]. Rutherford backscattering spectrometry (RBS) and X-ray Absorption Near Edge Structure (XANES) studies also suggested that the formation of such compounds is size sensitive and takes place during catalyst calcination [6,7]. Furthermore, detailed TPR and XANES studies pointed at the

formation of such compounds during catalyst reduction [8,9] and at the onset of Fischer–Tropsch synthesis [10].

Here reduction of a Re promoted Co/γ-Al_2O_3 catalyst was monitored *in situ* by synchrotron X-ray powder diffraction (XRPD) under H_2 environment. Whole powder pattern analysis revealed a non-linear expansion of the unit cell of γ-Al_2O_3 during the reduction process, suggesting diffusion of Co cations into the structure of the support. The non-linear cell expansion coincided with the formation of CoO phase. In addition, space resolved diffraction at the inlet and outlet of the reactor evidenced a negative effect of the partial pressure of indigenous $H_2O_{(g)}$ on the reduction process.

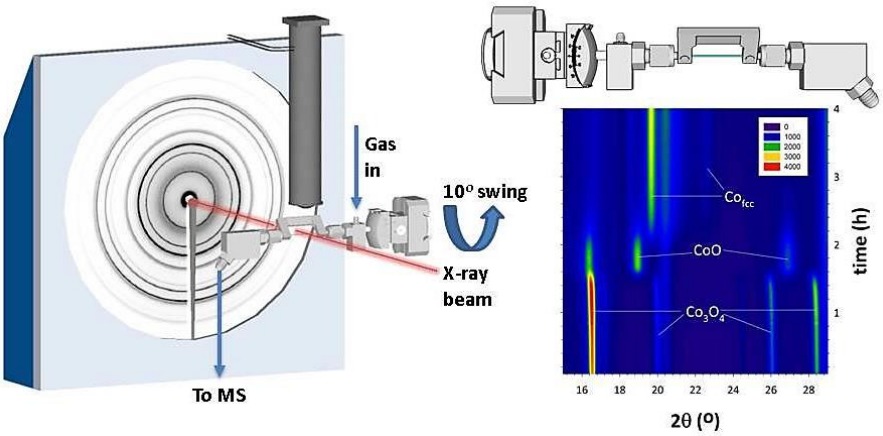

Figure 1. Representation of the used set-up (BM01A) configuration together with a 3D representation of the *in situ* cell and a contour plot of the obtained data set showing the main crystalline phases evolving during the course of reduction.

The catalyst used in this study consists of 20 wt% Co, 1 wt% Re supported on a high surface area γ-Al_2O_3. The catalyst was prepared by aqueous co-impregnation of $Co(NO_3)_2{\cdot}6H_2O$ and $HReO_4$. *In situ* XRPD measurements were performed at stations BM01A and BM01B of the Swiss-Norwegian Beamlines (SNBL) located at the European Synchrotron Radiation Facility (ESRF) in Grenoble, France. A quartz capillary based *in situ* cell has been used [11]. A vertical hot air blower heated the sample. Swing movement of a few degrees was applied for increased diffraction signal statistics (BM01A). A scheme of the experimental configuration together with the design of the cell and a contour plot of the acquired diffraction patterns can be seen (Fig. 1). The Co_3O_4 NPs were reduced by exposing the catalyst to a pure H_2 flow of 2.5 ml/min at ambient pressure, while the temperature was increased from 25 °C to 400 °C at 3 °C /min. The temperature was held at 400 °C for 4 hours (BM01A). For the TPR-XRPD experiment a temperature range from 100 to 700 °C was applied (BM01B).

At the examined temperature range and with the linear temperature ramp of 3 °C/min, a linear thermal expansion of the *γ*-Al_2O_3 support is expected [12]. Nevertheless, a sudden increase in the unit cell dimensions of *γ*-Al_2O_3 is observed at temperatures exceeding 190 °C. This deviation from linearity coincides with the formation of CoO (Fig. 2). The non-linear behaviour suggests that partial incorporation of Co^{2+} ions into the *γ*-Al_2O_3 lattice occurs. Extrapolation of the linear part at 270 °C and its comparison with the observed value at the same temperature reveals a 0.064 % increase in the lattice constant and an expansion of the unit cell volume equal to 0.19 % (Fig. 2).

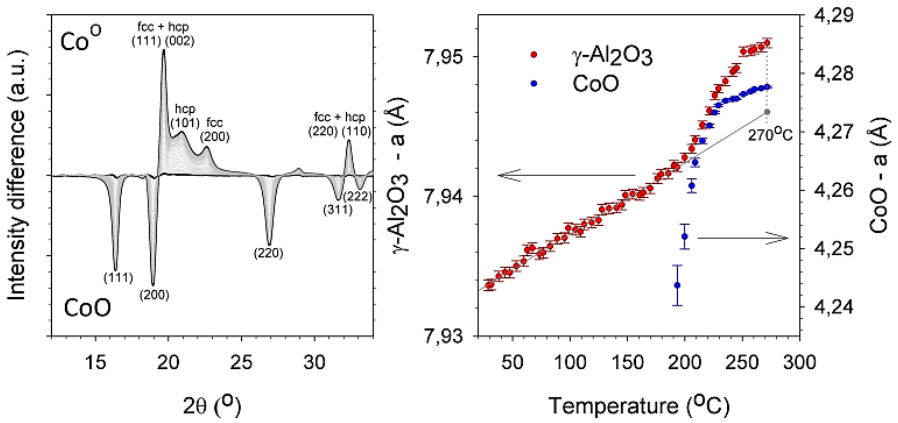

Figure 2. Normalised X-ray diffraction patterns from 250 °C to the reductions end, obtained by the subtraction of the diffractogram with CoO at maximum intensity (at 250 °C), showing the formation of metallic Co (top half) and disappearance of CoO (bottom half), (left). Variation in the lattice constant for γ-Al_2O_3 and CoO as a function of reduction temperature (right), λ = 0.7042 Å.

Line broadening analysis on the (440) reflection of γ-Al_2O_3 (not shown here) supports the above observation. Peak broadening occurs simultaneously with the formation of the CoO phase, suggesting that micro-strain is induced by Co diffusion and leads to cell expansion or the formation of a new phase. The transition from the amorphous to the crystalline CoO has an initial unit cell with a lattice constant of 4.243 Å. As the CoO crystallites grow, a significant expansion of the cell can be seen that cannot be merely explained by thermal effects. At about 225 °C the lattice parameter is stabilizing and further characterized primarily by the thermal expansion of CoO (Fig. 2).

It is suggested that diffusion of Co^{2+} cations takes place at sub-surface layers of *γ*-Al_2O_3 and grain boundaries of the 10 nm crystallites that are binned together, forming the γ-Al_2O_3 porous structure. Apparently, deeper diffusion of individual Co atoms into the *γ*-Al_2O_3 bulk also occurs. The interfacial area between Co NPs and the support may also provide a minor contribution to the observed expansion. Solid-state reactions of *γ*-Al_2O_3 with transition metal cations of low valence have previously been identified to proceed through counter-diffusion of metal in divalent state and Al^{3+} ions, yet at much higher temperatures and under O_2 rich environments [13].

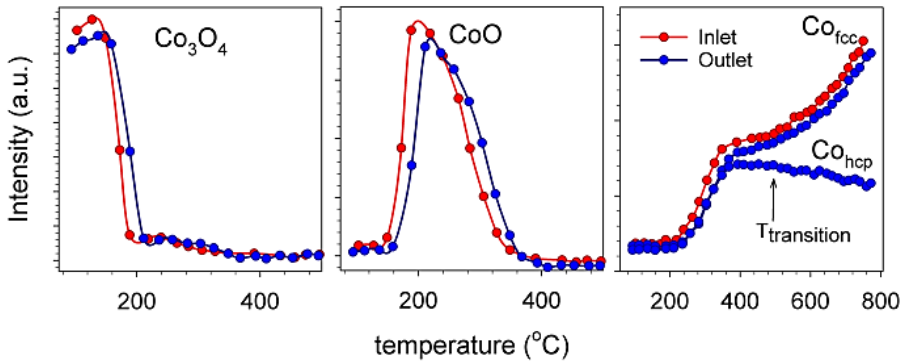

Figure 3. Peak Intensities of selected reflections for Co_3O_4 (220), CoO (220), hcp-Co (101) and fcc-Co (200) in the inlet and the outlet of the reactor, λ = 0.5052 Å.

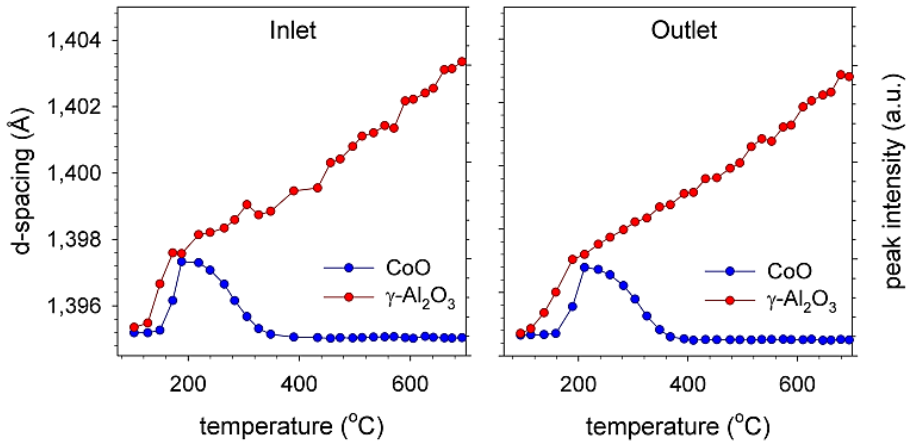

Figure 4. The d-spacing of (440) reflection of γ- Al_2O_3 (red) plotted together with the intensity of CoO (blue), λ = 0.5052 Å.

The reactor profile was analysed during catalyst reduction on a TPR-XRPD experiment (BM01B). Inlet and outlet were probed sequentially. The results are presented in Fig. 3 and Fig. 4. It becomes apparent from the steep increase at ca. 160 °C in the d-spacing for *γ*-Al_2O_3 that diffusion of Co^{2+} cations occurs in the entire length of the reactor during the reduction process. It is also observed that the phenomenon is irreversible, even at temperatures as high as 700 °C (Fig. 4). Besides, the reactor outlet exhibits a delay of the reduction process. The delay concerns both reduction steps. The CoO intermediate at the outlet reaches its highest intensity approximately 20 °C higher than the observed maximum for the inlet. The evolution of both fcc and hcp Co phases are equally delayed. Furthermore, the phase transition of metallic Co from the hcp to the fcc structure, although not well resolved in the current dataset, appears to occur at temperatures above 450 °C , temperature higher than the fcc → hcp transition of bulk Co or Co NPs supported on weakly interaction carbon [14]. This delay in transition temperature could be linked to the developed metal-support interactions.

Although the high temperature chemistry of this solid-state reaction resulting in a rich in Co^{2+} T_d crystalline $CoAl_2O_4$ spinel is reasonably known, the formation of the non-stoichiometric compounds that lack long range order under H_2 conditions is difficult to detect. Here we take advantage of the global information that is obtained from *in situ* synchrotron X-ray diffraction patterns and contains both the changes in the state of the catalytically active compound as well as in the support. The expansion of the unit cell of the γ-Al_2O_3 support is an indirect evidence of partial diffusion of Co^{2+} that takes place during the first step of the reduction process coinciding with the formation of Co^{2+} O_h. The Co-support interaction has been captured *in situ*. The observation supports the hypothesis of the existence of an amorphous Co containing layer covering major surface area of γ-Al_2O_3 after aqueous impregnation [15]. It has also been demonstrated that the overall reduction process is inhibited by $H_2O_{(g)}$ generated *in situ* during the process.

The present findings provide a better understanding of the nature and possible influence of the Co-support mixed compounds that form during H_2 activation on a Re/Co/γ-Al_2O_3 catalyst. Such synchrotron experiments can also aid investigations on catalyst preparation procedures that are aiming at minimizing losses of the active metal. Ultimately, optimization of reduction kinetics for the formation of a catalyst with balance between performance (high degree of reduction) and better stability

(sintering prevention, due to increased metal-support interactions) can be investigated further in light of the assessed onset of Co-support interactions.

References

[1] B.M. Vogelaar, a. D. van Langeveld, P.J. Kooyman, C.M. Lok, R.L.C. Bonné, J.A. Moulijn, Catal. Today 163 (2011) 20–26.
[2] E. Rytter, N.E. Tsakoumis, A. Holmen, Catal. Today 261 (2016) 3–16.
[3] B.M. Weckhuysen, Chem. Commun. (Camb). (2002) 97–110.
[4] H. Topsøe, B.S. Clausen, Appl. Catal. 25 (1986) 273–293.
[5] A. Voronov, N.E. Tsakoumis, N. Hammer, W. Van Beek, H. Emerich, M. Rønning, Catal. Today 229 (2014) 23–33.
[6] P. Arnoldy, J.A. Moulijn, J. Catal. 93 (1985) 38–54.
[7] R.L. Chin, D.M. Hercules, J. Phys. Chem. 86 (1982) 360–367.
[8] A.M. Hilmen, D. Schanke, A. Holmen, Catal. Letters 38 (1996) 143–147.
[9] A. Moen, D.G. Nicholson, M. Rnning, G.M. Lamble, J.-F. Lee, H. Emerich, J. Chem. Soc. Faraday Trans. 93 (1997) 4071–4077.
[10] N.E. Tsakoumis, J.C. Walmsley, M. Rønning, W. van Beek, E. Rytter, A. Holmen, J. Am. Chem. Soc. (2017) jacs.6b11872.
[11] N.E. Tsakoumis, A. Voronov, M. Rønning, W. Van Beek, Ø. Borg, E. Rytter, A. Holmen, J. Catal. 291 (2012) 138–148.
[12] W. Kollenberg, J. Margalit, J. Mater. Sci. Lett. 11 (1992) 991–993.
[13] P.H. Bolt, F.H.P.M. Habraken, J.W. Geus, J. Solid State Chem. 135 (1998) 59–69.
[14] N.E. Tsakoumis, R. Dehghan-Niri, R.E. Johnsen, A. Voronov, W. van Beek, J.C. Walmsley, Ø. Borg, E. Rytter, D. Chen, M. Rønning, A. Holmen, Catal. Today 205 (2013) 86–93.
[15] K. Larmier, C. Chizallet, P. Raybaud, Angew. Chem. Int. Ed. Engl. 54 (2015) 6824–6827.

Publication

N.E. Tsakoumis, R.E. Johnsen, W. van Beek, M. Rønning, E. Rytter, A. Holmen, *Chem. Commun*. **52** (2016) 3239.

How Crystallite Size Controls Reaction Path in Non-Aqueous Metal Ion Batteries: The Example of Sodium Bismuth Alloying.

Jonas Sottmann[a,*], Matthias Herrmann[a], Ponniah Vajeeston[a], Yang Hu[a], Amund Ruud[a], Christina Drathen[b], Hermann Emerich[c], Helmer Fjellvåg[a,*], David S. Wragg[a]

[a]*Department of Chemistry, University of Oslo, Blindern, P.O. Box 1033, 0315 Oslo, Norway*
[b]*European Synchrotron, 71 Rue des Martyrs, 38043 Grenoble, France*
[c]*Swiss–Norwegian Beamlines, European Synchrotron, 71 Rue des Martyrs, 38043 Grenoble, France*

Sodium-ion batteries (SIBs) may become an inexpensive alternative to lithium-ion batteries (LIBs) for large-scale stationary storage of energy generated by intermittent renewable sources. Wide-spread abundancy and low cost of Na makes this technology particularly attractive. Similarities in Li and Na chemistries should facilitate a fast and cost effective scale up of SIB technology.
The current options for suitable SIBs anode materials are limited because most known materials suffer from insufficient cycling stability and/or low energy density. Hard carbons were found to exhibit suitable properties for use in SIBs and are considered to be the anode material of choice for the first generation of SIBs [1]. However, relatively low gravimetric and volumetric capacities limit their energy densities and low voltage operation raises concerns about Na metal deposition which is associated with safety hazards.
Alloying anodes (e.g. P, Sn, Sb, Bi) are a promising class of anode materials because they allow each anode atom to combine with several charge carriers, yielding high volumetric and gravimetric capacities. Despite the fact that improved performance has been observed for alloying anode materials made of nanoparticles, the reasons for the improvement are not fully understood [2].
Lithiation and sodiation mechanisms for Bi have been reported. The lithiation of Bi follows sequential formation of LiBi and Li_3Bi according to the Li–Bi equilibrium phase diagram which is fully reversible upon delithiation [3]. Reports on the sodiation mechanism for Bi are inconsistent. Ellis *et al.* reported that the sodiation and desodiation mechanisms reversibly follow the Na–Bi equilibrium phase diagram with the formation of NaBi and Na_3Bi [4]. Su *et al.* suggested Na intercalation in between Bi layers along the c-axis based on *ex situ* XRD [5].

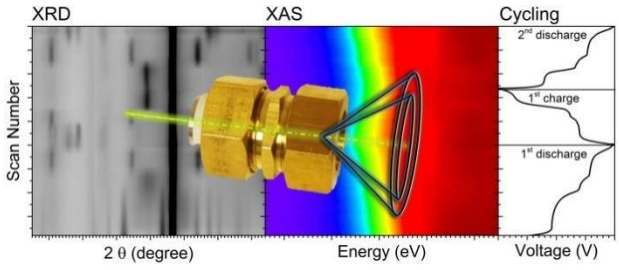

Figure 1. Illustration of the X-ray transparent electrochemical cell and its use for combined XRD/XAS *operando* studies of LIBs/SIBs at SNBL [6].

In this work we used our newly established set-up (X-ray transparent electrochemical cells, sample changer and interfacing software) for combined XRD/XAS *operando* studies of LIBs/SIBs at SNBL (Fig. 1) [6] to reinvestigate the working mechanism of Bi as a SIB alloying

anode material. It is important to clarify the sodiation mechanism for Bi since it is intimately linked with the cycling performance of the materials. Furthermore, it is crucial to identify factors (e.g. crystallite size, charge rate) that may influence the sodiation mechanism.

Micro- and nanocrystalline Bi carbon composites (Bi/C) were obtained using different ball milling conditions. The working electrodes are composed of Bi/C, additional conductive carbon black and poly(acrylic acid) (PAA) as binder, deposited on Al foil. Na metal was used as a counter electrode. Working and counter electrodes are separated by glass fibers soaked with electrolyte. The *operando* cell is used in transmission mode meaning that the X-rays travel through and interact with the all battery components. Galvanostatic cycling is performed under identical conditions with respect to the home laboratory electrochemical characterization in coin cells.

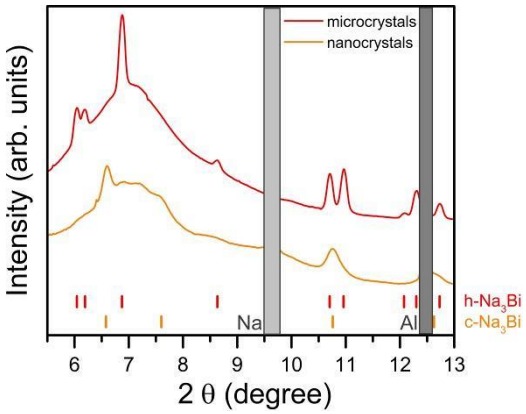

Figure 2. *Operando* XRD profiles (λ = 0.50648 Å) of micro- and nanocrystalline Bi anodes in discharged state (0 V). Tick marks indicate positions of Bragg reflections for hexagonal and cubic Na_3Bi phases. The gray bars mask reflections from Na and Al.

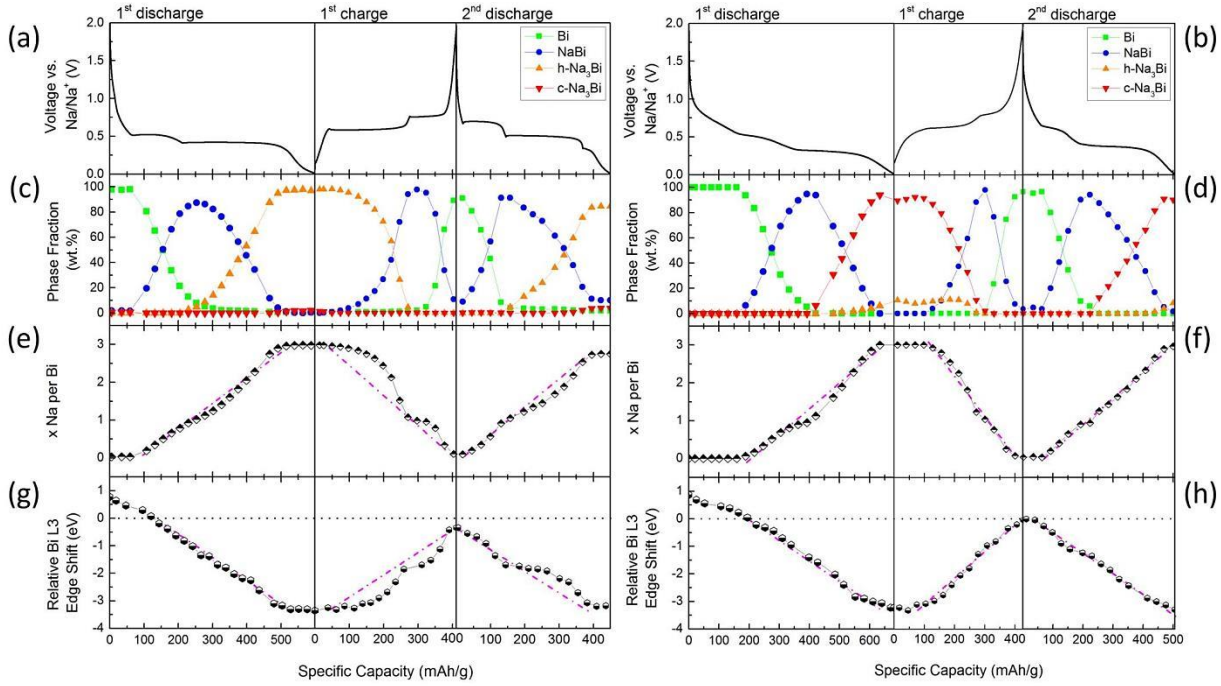

Figure 3. (a/b) Voltage profile of micro-/nanocrystalline Bi anodes compared to (c/d) phase fractions of Na-Bi phases, (e/f) number of Na per Bi calculated from the phase fractions and (g/h) the relative shift in Bi L_3 absorption edge position with respect to metallic Bi (13419 eV) for the first 1.5 galvanostatic cycles. The relative edge shift is initially positive due to presence of Bi_2O_3. A shift in the absorption edge position of an element to lower (higher) energies corresponds to a decrease (increase) of its average oxidation state.

Our results clearly show that in a nanostructured Bi anode the final Na_3Bi phase has a cubic structure (c-Na_3Bi), while for an anode containing microcrystalline Bi, hexagonal Na_3Bi (h-Na_3Bi) is formed (Fig. 2). The cubic Na_3Bi phase was previously only found at high pressures [7]. In both cases crystalline NaBi was found as an intermediate phase between the fully desodiated and sodiated forms. The voltage profiles for the first three (dis)charge steps of the two samples are shown in Fig. 1 alongside the *operando* XRD (phase fractions, number of Na per Bi) and XANES (Bi L_3-edge position) results. The Rietveld XRD results were obtained by refining each series of powder patterns in parallel as a single dataset [6]. Our results on the reaction path of the microcrystalline Bi reversibly following the Na–Bi equilibrium phase diagram are in good agreement with the *in situ* study by Ellis *et al.* [4]. The Na intercalation mechanism in between Bi layers suggested based on *ex situ* XRD data by Su *et al.* [5] was not observed for either microstructure.

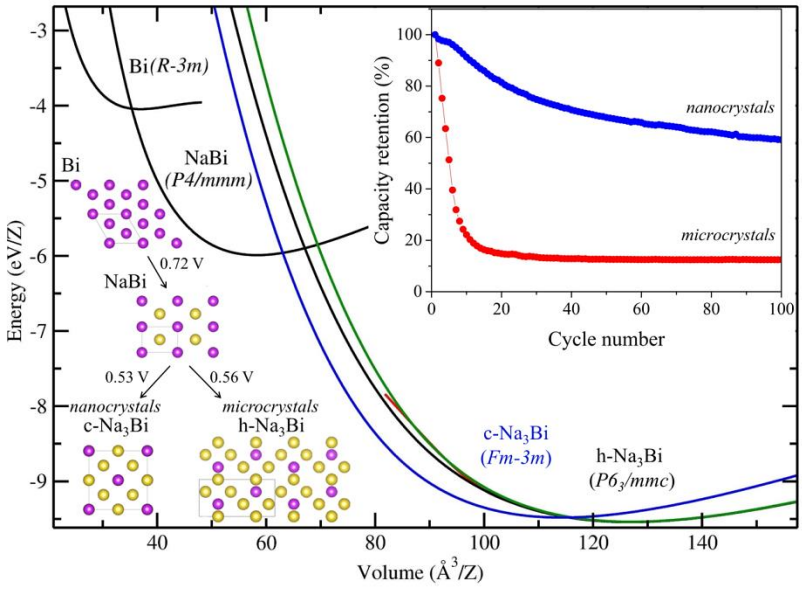

Figure 4. Illustration of the different structural and electrochemical pathways in the Na-Bi system and corresponding calculated total energy as a function of volume for the Na-Bi phases. c-Na_3Bi was found to be metastable, while the different polymorphs of h-Na_3Bi cannot be distinguished in terms of energy (difference ≤4 meV/Z) or using XRD. The inset shows the superior capacity retention of nanocrystalline vs microcrystalline Bi with cycle number.

The working mechanisms for micro- and nanocrystalline Bi are illustrated in Fig. 4. DFT calculations found c-Na_3Bi metastable to the polymorphs of h-Na_3Bi. Micro- and nanocrystalline Bi anodes form different amounts of c-Na_3Bi (4 wt. % and 92 wt. %, respectively). c-Na_3Bi is clearly favored in the sample with larger surface area of the nanocrystals which indicates that nucleation and growth of c-Na_3Bi occurs on the crystallite surfaces.

Comparison of the structures rationalizes why this leads to improved cycling stability (inset Fig. 4): the conversion path between NaBi and the cubic form requires fewer and smaller structural changes in terms of chemical bonds and volume changes. This hypothesis is supported by the deviation of the microcrystalline Bi anode from a linear change in Na/Bi ratio with progression of the alloying/de-alloying reactions

during discharge/charge (Fig. 3e) which is not observed for the nanocrystalline Bi anode (Fig. 3f). The change in Bi oxidation state, *i.e.* the Bi L_3 edge shift, mirrors the trends in Na/Bi ratios (excepts for the X-ray amorphous Bi_2O_3 present during the first discharge) for both Bi anodes (Fig. 3g and 3h) and thereby confirms that no X-ray amorphous intermediate Na_xBi phases were omitted in our XRD analysis.
The capacity degradation in the microcrystalline anode was attributed to the particle pulverization (cracking of the crystallites) revealed by *ex situ* XRD analysis after prolonged cycling: Particle pulverization reduces the particle-to-particle contacts which are essential for maintaining electronic conductivity in the electrode and is accompanied by the formation of inactive residuals (*i.e.* originally active particles trapped inside an inactive matrix) which leads to loss of capacity with cycle number.
Our study shows that crystallite size effects can influence the performance of battery materials by making the structural chemistry deviate from what is predicted by the equilibrium phase diagram. Using crystallite size to direct the structural chemistry we may thus be able to improve the lifetime of high capacity batteries effectively and at low cost.
In continuation of our work on Bi based anodes we investigated the reaction and degradation mechanisms of Bi_2S_3 as conversion-type anode [6]; and discovered $BiVO_4$ and $Bi_2(MoO_4)_3$ as representatives of a novel class of high performance SIB anodes. For the latter, we will report in our forthcoming publication [8] that the initial compounds are irreversibly converted into alloying Bi nanocrystallites confined in a matrix of electrochemically active insertion hosts $Na_{3+x}VO_4$ and $Na_{2+x}MoO_4$, respectively. The nanostructured composite anode thus obtained has excellent high rate performance and retains its capacity over hundreds of cycles.

References

[1] E. Irisarri, A. Ponrouch and M. R. Palacin, *J. Electrochem. Soc.* **162** (2015) A2476.
[2] D. Larcher, S. Beattie, M. Morcrette, K. Edstrom, J.-C. Jumas and J.-M. Tarascon, *J. Mater. Chem.* **17** (2007) 3759.
[3] W. Xianming, T. Nishina and I. Uchida, *J. Power Sources* **104** (2002) 90.
[4] L. D. Ellis, B. N. Wilkes, T. D. Hatchard and M. N. Obrovac, *J. Electrochem. Soc.* **161** (2014) A416.
[5] D. Su, S. Dou and G. Wang, *Nano Energy* **12** (2015) 88.
[6] J. Sottmann, R. Homs-Regojo, D. S. Wragg, H. Fjellvåg, S. Margadonna and H. Emerich, *J. Appl. Crystallogr.* **49** (2016) 1972.
[7] M. E. Leonova, I. K. Bdikin, S. A. Kulinich, O. K. Gulish, L. G. Sevast'yanova and K. P. Burdina, *Inorg. Mater.* **39** (2003) 266.
[8] J. Sottmann, M. Herrmann, P. Vajeeston, A. Ruud, C. Drathen, H. Emerich, D. S. Wragg and H. Fjellvåg, submitted to *Chem. Mater.*

Publication

J. Sottmann, M. Herrmann, P. Vajeeston, Y. Hu, A. Ruud, C. Drathen, H. Emerich, H. Fjellvåg and D. S. Wragg, *Chem. Mater.* **28** (2016) 2750.

Nanoporous Intergrowths: how crystal growth dictates phase composition and hierarchical structure in the CHA/AEI system

Rachel L. Smith,[a] Wojciech A. Sławiński,[b,d] Anna Lind,[c] David S. Wragg,[b] Jasmina H. Cavka,[c] Bjørnar Arstad,[c] Helmer Fjellvåg,[b] Martin P. Attfield,[a] Duncan Akporiaye[c] & Michael W. Anderson[a]

[a] *Centre for Nanoporous Materials, School of Chemistry, The University of Manchester, Oxford Road, Manchester, M13 9PL, UK*
[b] *Centre for Materials Science and Nanotechnology, Department of Chemistry, University of Oslo, PO Box 1126, 0315 Oslo, Norway*
[c] *SINTEF Materials and Chemistry, PO Box 124, Blindern, 0314 Oslo, Norway*
[d] *On leave from Institute of Experimental Physics, University of Warsaw, Pasteura 5, 02-093 Warsaw, Poland*

Some of the most important nanoporous materials in industrial applications are formed as intergrowths between structurally related phases. Further, the specific properties and functions are often strongly related to the nature of these intergrowths. By their nature such structures are notoriously difficult to characterize in detail and thereby formulate a structure/property relationship. We approached the problem of the industrially relevant CHA/AEI intergrowth system by not only getting insight into the structure of the materials but also the crystal-growth mechanism and show that the former is crucially dependent upon the latter.

Silicoaluminophosphate SAPO-34 is a widely used catalyst in the Methanol-to-Olefins (MTO) process. [1] SAPO-34 gives a high selectivity to light olefins (C2-C3) and high conversion rates due to the small pore aperture (3.8 Å) and appropriate high acid site density. [2] One of the main challenges with the SAPO-34 catalyst is rapid deactivation due to coke formation. [3] The related material SAPO-18 is a potential MTO catalyst and typically has a lower acid site density and lower acid strength, hence a lower activity but longer lifetime, than SAPO-34. [4,5] CHA/AEI intergrowths are reported in the patent literature as desirable catalysts for the MTO reaction and can be more stable to deactivation than pure-phase SAPO-34. [6-8] However, the structures of these intergrowths are difficult to characterize and are poorly understood.

SAPO-34 has the same framework type, CHA, as the zeolite chabazite. [9] The framework can be considered as layers of tilted double 6-rings (D6Rs), all with the same orientation, in an AAAA… stacking pattern (Figure 1a, grey). Here, these layers will be referred to as the common repeat layer. The stacking of these D6Rs gives rise to the large, internal CHA cage (Figure 1, orange). The related material SAPO-18, framework type AEI, is built of the same common repeat layers but stacked in an ABAB… pattern, leading to an alternation in the orientation of the D6Rs in the [001] direction (Figure 1, white and grey shows the alternating orientation of the D6Rs).10 This gives a different internal cage type, the AEI cage (Figure 1, blue). The AEI cages also alternate in direction every half-unit cell due to the differences in the D6R stacking. Since the (001) surface of SAPO-18 is isostructural with SAPO-34, it is possible to form intergrowths of the two phases in the [001] AEI direction (figure 1 , bottom). However, these CHA/AEI intergrowths are not as well understood as the SAPO-34 and SAPO-18 end-members. It is important to understand the formation of these intergrowths in order to understand their improved catalytic activity for the MTO process.

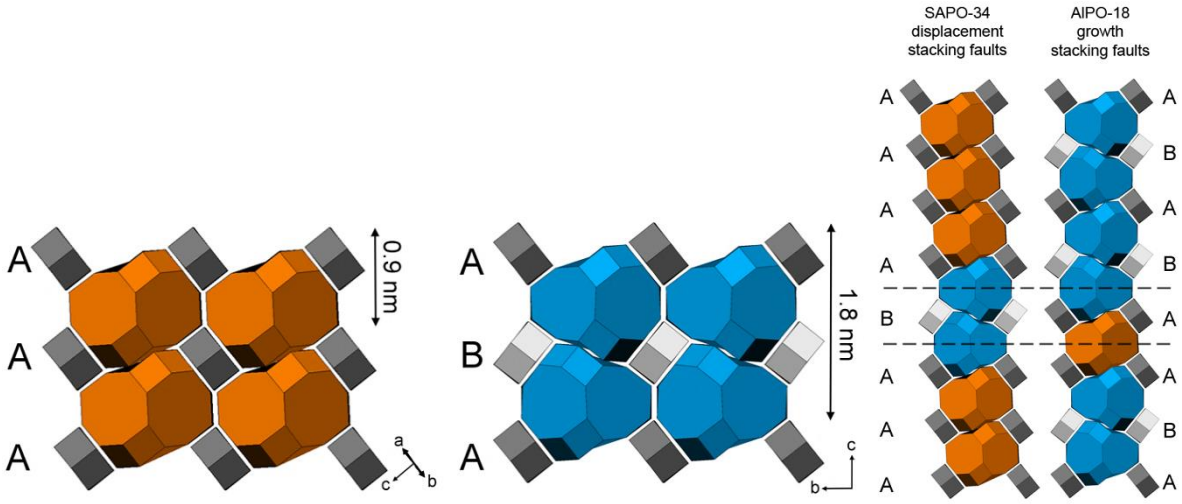

Figure 1. Framework structure of SAPO-34 (top left) and SAPO-18 (top right), showing the orientation of the tilted D6Rs and the difference in layer stacking and internal cage type. Below we see the two possible types of stacking fault which can occur in the structures

Using a combination of XRD, NMR and AFM we have managed to fully characterise these intergrowths. A series of CHA/AEI intergrowth materials were synthesized by varying the silicon ratio in the synthesis gel. Typically, low levels of silicon result in SAPO-18 and increased levels of silicon prompt SAPO-34 formation.15 A sequential increase in silicon content from 0.0% to 7.0% silicon was used to synthesize a series of materials with a gradual change from AEI to CHA character.

Using data collected on the high resolution powder diffractometer at beamline BM01B analysed with the method developed by Slawinski [9] et al in the program DISCUS [10] we characterised the full series of samples in terms of phase fractions, levels of intergrowth and number of layers of CHA/AEI type cages (figure 2). NMR spectra of the as synthesised materials allowed us to differentiate the CHA cages from the AEI cages, giving a measure which shows a striking correlation with the XRD results (figure 2).

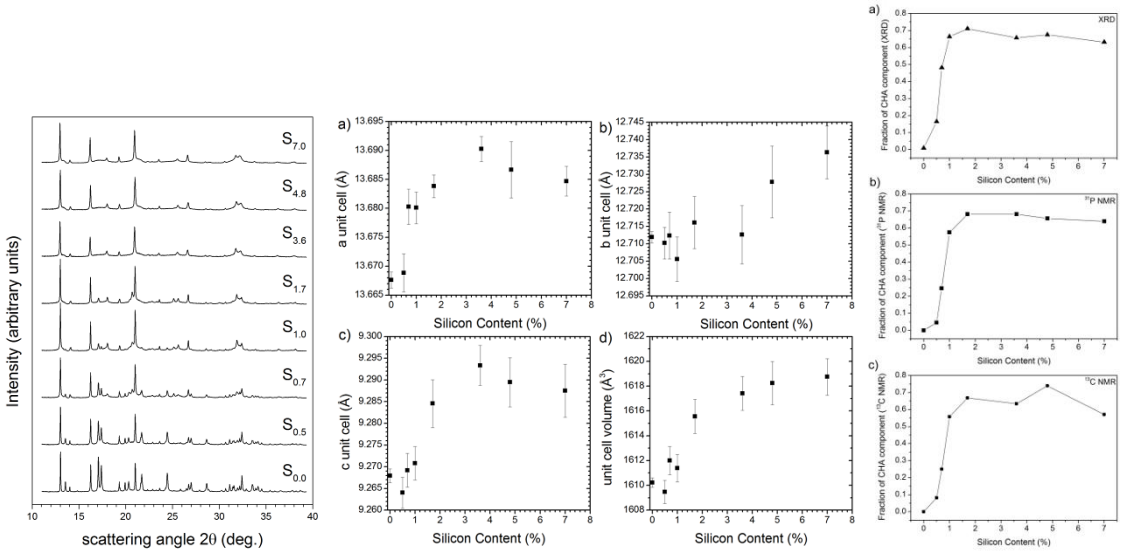

Figure 2. Powder diffraction patterns for the sample series (left) and unit cell dimensions for the layered model in DISCUS (centre). The unit cell expands as silicon content increases and phosphorus is replaced in the framework by larger silicon atoms. (Right) correlation between the fraction of CHA-type cages found by XRD, ^{31}P and ^{13}C NMR.

With AFM we can clearly see features related to AEI, CHA and intergrowth structures. Our analysis suggests that the low-energy spiral growth mechanism promotes the formation of the defect-free end members, while intergrowths form in a layer-by layer process, with spiral growth being prevented in the intergrowths by the incompatibility of the CHA and AEI growth spirals (figure 3).

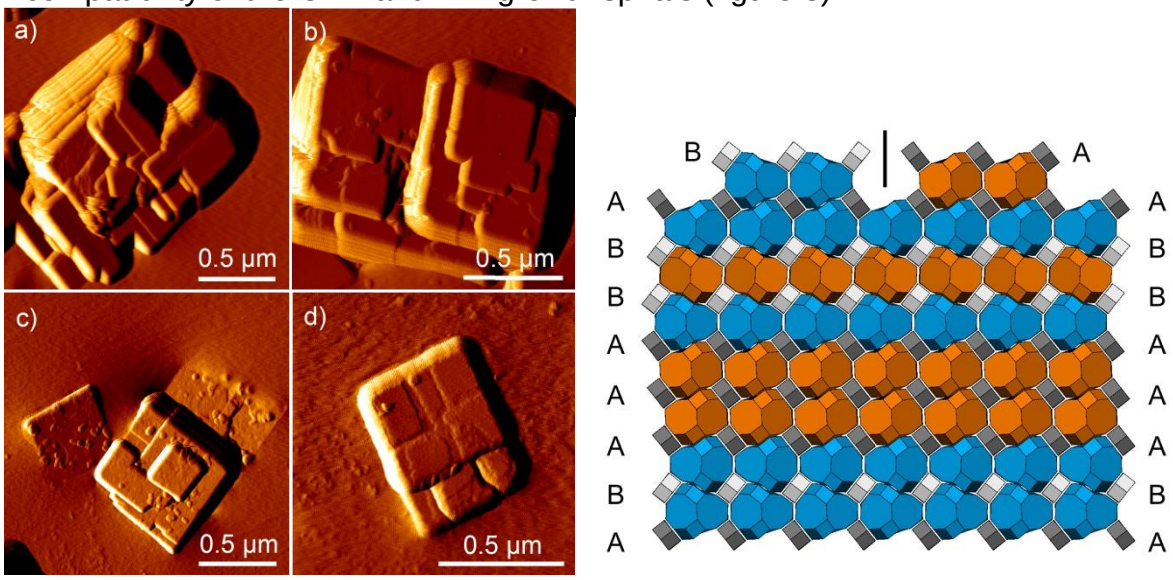

Figure 3. AFM vertical deflection images of selected typical intergrowth crystals; a-b) $S_{3.6}$; c) $S_{7.0}$; d) $S_{1.7}$ (left) and a model showing an intergrowth crystal with incompatible CHA and AEI spirals forming on the surface (right).

The crystal-growth observations, combined with insight from XRD and NMR data, reveal important characteristics and complexity of the CHA/AEI system. Awareness of fundamental crystal growth is important since the competing crystal-growth mechanisms can have profound effects on the final structure of intergrowths and thus can have a large effect on their function and applications. Many zeotype systems form intergrowths that are traditionally viewed as a switching of layer stacking. However, this is not possible if the crystal grows by spiral growth around a screw dislocation. Consequently, this possibility must always be considered and, where possible, investigated. Finally, an understanding of the growth of these materials gives future opportunities for control of intergrowth formation and the possibility to tailor the desired catalytic properties [11].

References

[1] Chen, J. Q.; Bozzano, A.; Glover, B.; Fuglerud, T.; Kvisle, S. Catal. Today. 106 (2005) 103–107
[2] Vora, B. V.; Marker, T. L.; Barger, P. T.; Nilsen, H. R.; Kvisle, S.; Fuglerud, T. Stud. Surf. Sci. Catal. 107 (1997) 87-98
[3] Chen, D.; Moljord, K.; Holmen, A. Microporous Mesoporous Mater. 164 (2012) 239–250
[4] Djieugoue, M.-A.; Prakash, A. M.; Kevan, L. J. Phys. Chem. B. 104 (2000) 6452-6461
[5] Aguayo, A. T.; Gayubo, A. G.; Vivanco, R.; Olazar, M.; Bilbao, J. Appl. Catal., A. 283 (2005) 197–207

[6] Wendlebo, R.; Akporiaye, D. E.; Anderson, A.; Dahl, M. I.; Mostad, H. B.; Fuglerud, T.; Kvisle, S. U.S. Patent 6,334,994, January 1, 2002
[7] Sinkler, W.; Broach, R. W.; Erdman, N.; Reynolds, T. M.; Chen, J. Q.; Wilson, S. T.; Barger, P. T. U.S. Patent 7,547,812, June 16, 2009
[8] Mertens, M. M. WO 2009/117186, February 6, 2009
[9] Sławiński, W. A.; Wragg, D. S.; Akporiaye, D.; Fjellvåg, H. Microporous Mesoporous Mater. 195 (2014) 311-318
[10] Proffen, T.; Neder, R. B. Appl. Crystallogr. 30 (1997) 171-175
[11] Smith R.L., Svelle S., del Campo, P., Fuglerud, T., Arstad, B., Lind, A., Chavan, S., Attfield, M.P., Akporiaye, D., Anderson, M.W. Applied Catal. A, 505, (2015), 1-7

Publication

Smith, R. L., Sławiński, W.A., Lind,A., Wragg, D.S., Cavka, J.H., Bjørnar Arstad, B., Fjellvåg, H., Attfield, M.P., Akporiaye, D., Anderson, M.W. (2015) "Nanoporous Intergrowths: How Crystal Growth Dictates Phase Composition and Hierarchical Structure in the CHA/AEI System." Chem. Mater. **27**(12): 4205-4215.

STATUS OF FACILITY

BM01

The main activity on BM01 is on studying structure and functional response of various materials ranging from pharmaceutically relevant crystals to compound used in energy-related research. Instrumentation development targeted at *in-situ* experiments has also been an important aspect of the beamline work in recent years, particularly for studying ferroelectric materials, materials for electrochemical and hydrogen storage applications. The main instrument is a multifunctional diffraction platform based on PILATUS 2M detector together with very flexible and versatile diffraction goniometry. The diffraction experiment is controlled by a SNBL-developed software Pylatus that also controls numerous sample environment tools (heaters, coolers, cryostat, user-supplied sample cells). Most of the development activities in 2015-2016 have been concentrated on exploiting the full potential of the system. The diffractometer equipped with the PILATUS detector is shown in Fig. 1.

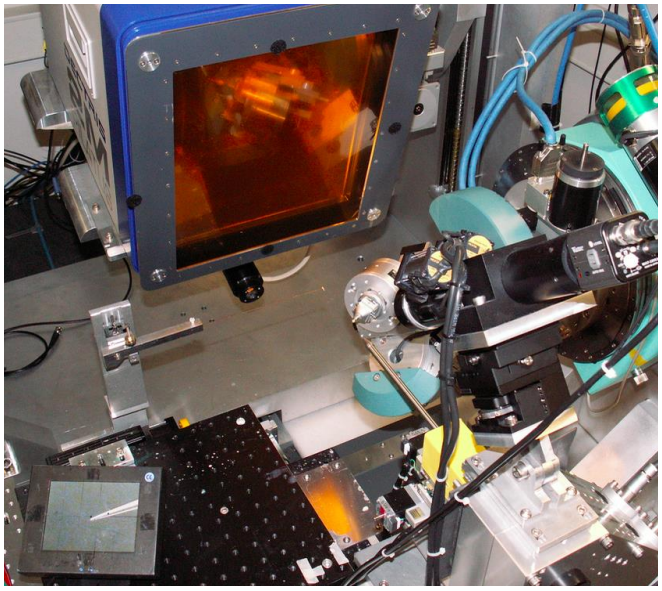

Figure 1. Layout of the PILATUS@SNBL diffractometer set for a single crystal experiment.

We have also developed new data processing tools that optimize the use of the beam time and simplify further data processing. Recent versions of SNBL ToolBox, BUBBLE and MEDVED are available for users at www.snbl.eu. The list of available options, specifications, and software tools are described in the beamline paper [Dyadkin, V., Pattison, Ph., Dmitriev, V., Chernyshov, D. A new multipurpose diffractometer PILATUS@SNBL *J. Synchrotron Rad*., **23**, 3, 2016], see also Fig. 2.

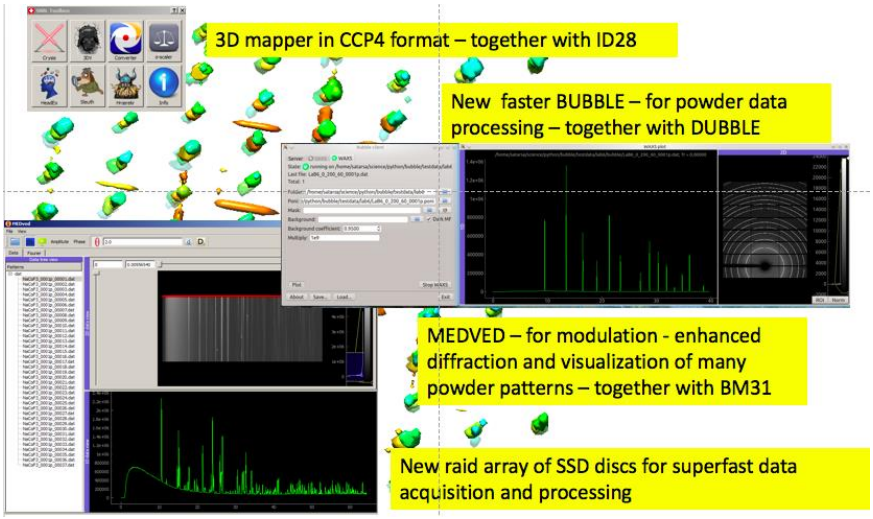

Figure 2. New software tools now avalaible for SNBL users: SNBL ToolBox, BUBBLE, and MEDVED.

One of the scientific areas for which the new equipment provides significant advantages is the investigation of diffuse X-ray scattering in single crystals with a certain degree of disorder. Diffuse scattering data collected at BM01 were used to study such disorder phenomena in a high entropy refractory alloy [Maiti, S., Steurer, W. Structural-disorder and its effect on mechanical properties in single-phase TaNbHfZr high-entropy alloy *Acta Materialia*, **106**, 87–97, 2016]. This study reveals the details of the structural disorder, a mechanism of evolution of the disorder with annealing and resulting effects on the mechanical properties at ambient temperature.

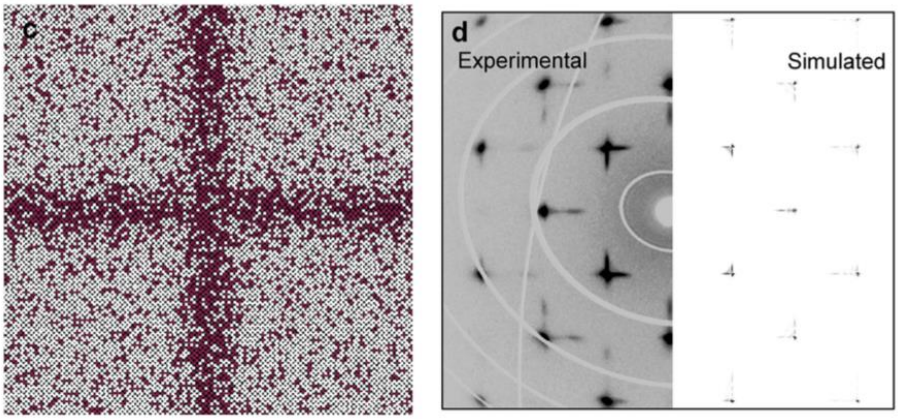

Figure 3. A disordered model structure (left), experimental and simulated scattering patterns (right) for a high entropy alloy [Acta Materialia, **106**, 87–97, 2016]

The diffraction platform at the beamline has also been used for the structure solution of new materials [Ovsyannikov, S.V., Bykov, M., Bykova *et al*. Charge-ordering transition in iron oxide Fe_4O_5 involving competing dimer and trimer formation, *Nature Chemistry*, **8**, 501-508, 2016; Øygarden, V., Fjellvåg, H., Sørby, M.H., Sjåstad, A.O. Crystal Structure of $LaSr_3Fe_3O_8(OH)_2{\cdot}xH_2O$ *Inorg. Chem.*, **55**, 15, 7630-7636, 2016], for structural characterization of materials with interesting magnetic and transport properties

[Ansermet, D., Petrovic, A.P., He, Sh., Chernyshov, D. *et al.* Re-entrant Phase Coherence in Superconducting Nanowire Composites, *ACS Nano*, **10**, 515-523, 2016], for studying physics and chemistry of battery materials [Monchak, M., Hupfer, Th., Senyshyn, A. *et al.* Lithium Diffusion Pathway in $Li_{1.3}Al_{0.3}Ti_{1.7}(PO_4)_3$ (LATP) Superionic Conductor, *Inorg. Chem.*, **55**, 2941-2945, 2016]. Notably, in all above papers our users combine the diffraction experiments at BM01 with other experimental probes, such as neutron diffraction, spectroscopy and characterization of macroscopic properties.

In these and similar studies, it is not only the excellent characteristics of the new PILATUS@SNBL diffractometer but rather a combination of different experimental probes that opens up many exciting avenues of research in the fields of solid state physics and crystal chemistry. An *in-situ* synchrotron diffraction experiment that offers not only structure but a functional response of the material at the microscopic level is the key ingredient of all the above examples.

Future developments on the beamline

The relocation of BM01B onto BM31 bending magnet port of the ESRF offered some free place for the further development of the BM01 station. However, our main priority is to prepare for the ESRF upgrade that would offer us much more intense beam. The ESRF machine upgrade to a new lattice will replace existing bending magnet with a 2-pole Wiggler source. The existing optics has to be modified in order to handle the higher thermal load and to optimize its use with the new source. We have therefore already started an upgrade of the existing monochromator with IDT Ltd. (UK) (Fig. 4). The delivery and installation are planned for 2018.

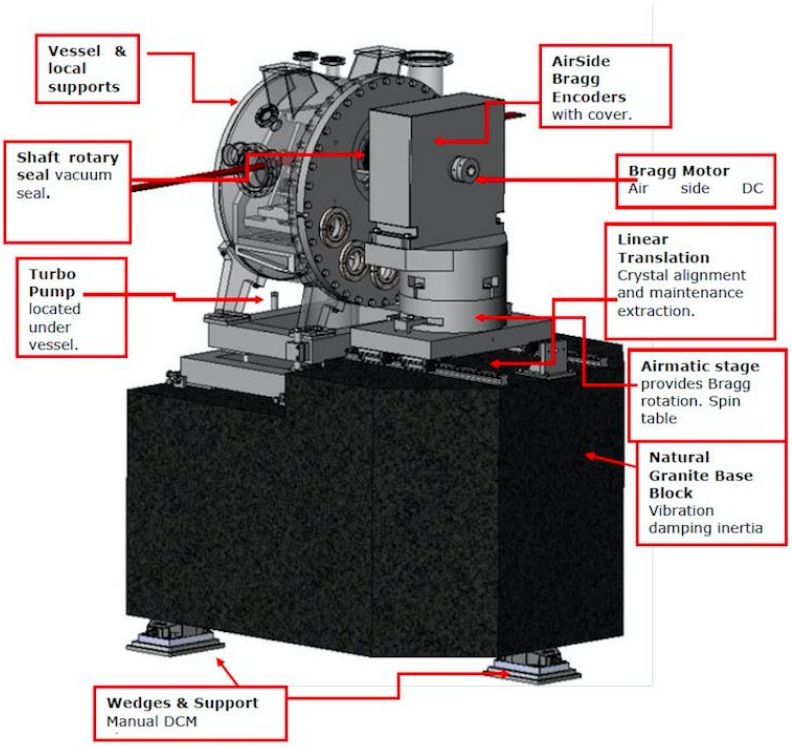

Figure 4. New monochromator for BM01 constructed by Instrument Design Technology Ltd. UK.

Concerning the further development of PILATUS@SNBL, considerable effort is now focused on the organization, processing and storage of the very large amounts of data generated by a typical experiment. In order to define the extent of the problem, and the demands on new software required for streamlined data processing, a joint **ESRF/SNBL workshop ("Big data for small molecule crystallography")** was held in 2015. In another area of technical improvements, the staff of SNBL is collaborating with Dectris Ltd. Together with the Dectris team and researchers from University of Siegen (Germany) we have carried out a test of a new detector Eiger X 500K that has 9kHz readout frequency. The detector has been used for pioneering experiments on how a fast switching electric field affects the domain distribution in a ferroelectric crystal which in turn explains the macroscopic properties. These results provide unique new insights and show the potential of the setup. Such a fast detector installed on PILATUS@SNBL; in combination with large area Pilatus2M would allow for time resolved diffraction combined with reciprocal space mapping. Hence the permanent installation of this fast detector would significantly contribute to the unique capabilities of BM01 and is a highly desired upgrade path.

From BM01B to BM31

Powder Diffraction and EXAFS Station

Current status

2016 has been a turning point in the history of the former SNBL B-Station where a long standing wish has become reality.
So-far further developments of the SNBL station dedicated to Powder Diffraction (PD) and EXAFS has been hampered by the reduced space due to the vicinity of the second SNBL beamline, BM01A. In past negotiations with our Swiss and Norwegian funding agencies and the ESRF we got the permission in June 2014 to move our existing beamline BM01B to a new and independent ESRF bending magnet port: BM31.
This implied the design of new lead hutches and data acquisition cabins, followed by a call for tender and eventually the construction of the hutches and infrastructure in autumn 2015/spring 2016 already.
In summer 2016 we moved all our beamline components and equipment to the newly constructed lead hutches. In an effective down time of 3 months only, the components could be moved to the 'new' beamline where they were aligned and commissioned.
BM31 opened its doors for normal user operation again at the 20th of September 2016 and is fully operational again since.

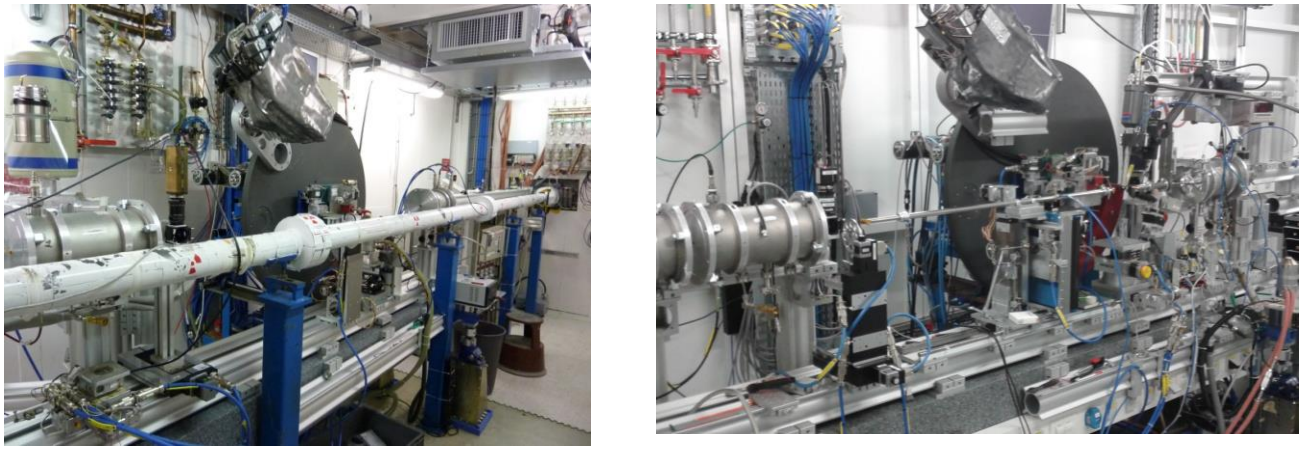

Figure 5. Picture of similar view:
Former BM01B station (left) and the new BM31 experimental station (right).

Comparing the left and the right picture, one can see that the space (and access) formerly taken by the A-line (white piping) is now free.

The next picture show that all construction works are finished and that the new beamline is fully operational.

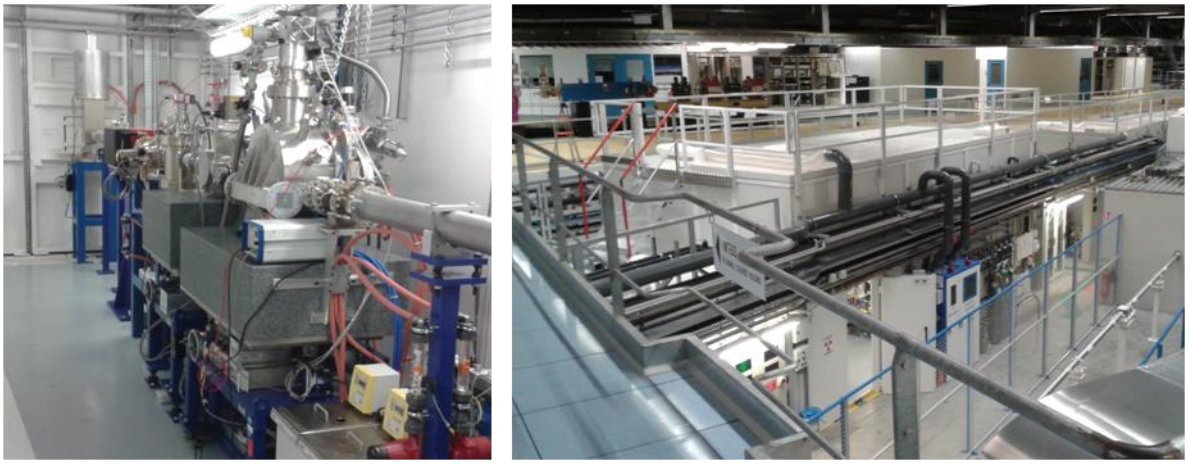

Figure 6. (Left) New BM31 optics enclosure and optical components. (Right) New hutches as seen from the bridge linking the Central Building with the machine control room

Scientific results

Despite the complete removal and reconstruction of the entire beamline and the resulting 3 month down-time, the scientific output has remained at very high level in 2016.

The battery set-up as described in the last years report has led to several publications and continues to be heavily used. A detailed description of the new set-up has been published in "Journal of Applied Crystallography" (2016) under the title "*Versatile electrochemical cell for Li/Na-ion batteries and high-throughput setup for combined operando X-ray diffraction and absorption spectroscopy*". The paper describes the electronic and structural changes in high-voltage Li insertion cathode material $LiMn_{1.5}Ni_{0.5}O_4$ and high-capacity sodium conversion anode material Bi_2S_3 during cycling. In the study, where - upon (dis)charging - powder diffraction data, EXAFS and galvanic data have been collected in a quasi-simultaneous way, it became clear that for the Bi_2S_3 compound one can assign a partially reversible redox reaction to the (de)sodiation: $Bi_2S_3 + 12Na \leftrightarrow Na_3Bi + 3NaS$.

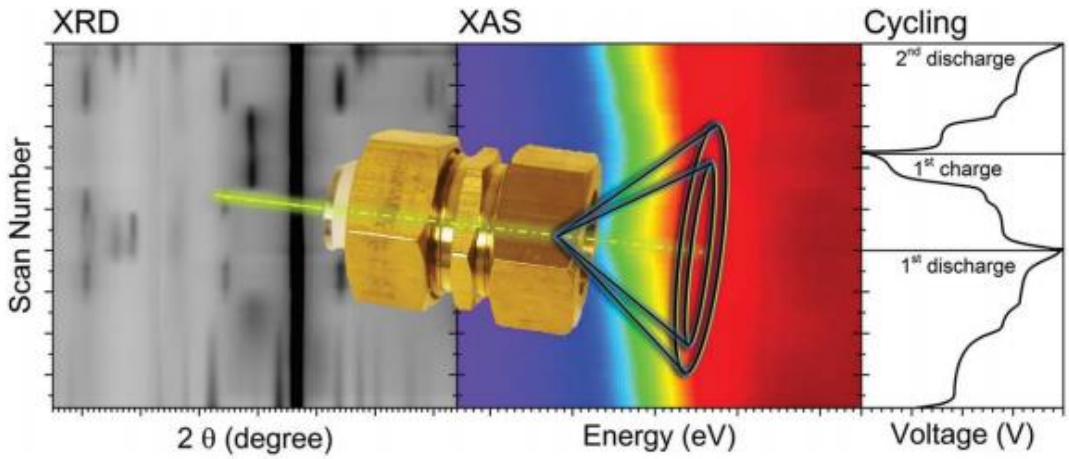

Figure 7. Measurements performed during charging and discharging of the cell.
Left: Film plot of the background-subtracted diffraction profiles (λ= 0.5Å); Centre: Evolution of the Bi-L_3 edge XANES spectra collected quasi-simultaneously; Right: The voltage profile upon charging and discharging.

One result of the study is that the crystallites (initially a few nm in size) grow with increasing cycling number. The larger Bi particles provide less interfacial surface at which the sulfurization of Bi can take place reversibly. The capacity fading can be seen as a result of the irreversibility of the Bi_2S_3 conversion reaction, as shown by the reduction of the Bi_2S_3 phase fraction formed at the end of each cycle. For a reversible operation it is thus crucial to maintain the metal to non-metal.
A similar study appeared in "Electrochimica Acta" under the title "*In operando Synchrotron XRD/XAS Investigation of Sodium Insertion into the Prussian Blue Analogue Cathode Material: $Na_{1.32}Mn[Fe(CN)_6]_{0.83}$* z H_2O*". Again, powder diffraction and EXAFS data have been collected on BM01B during charging and discharging and the simultaneous collection of galvanostatic data. Thus the charge state could be linked to structural and electronic properties of this material.

Upon (de)sodiation it was found that the Prussian Blue Analogue (PBA) adopts three different phases (A,B,C). Literature and measurements suggest a cooperative displacement of the Na-ions via dipole-dipole interactions along the cubic [111] direction as being at the origin of this transformation.

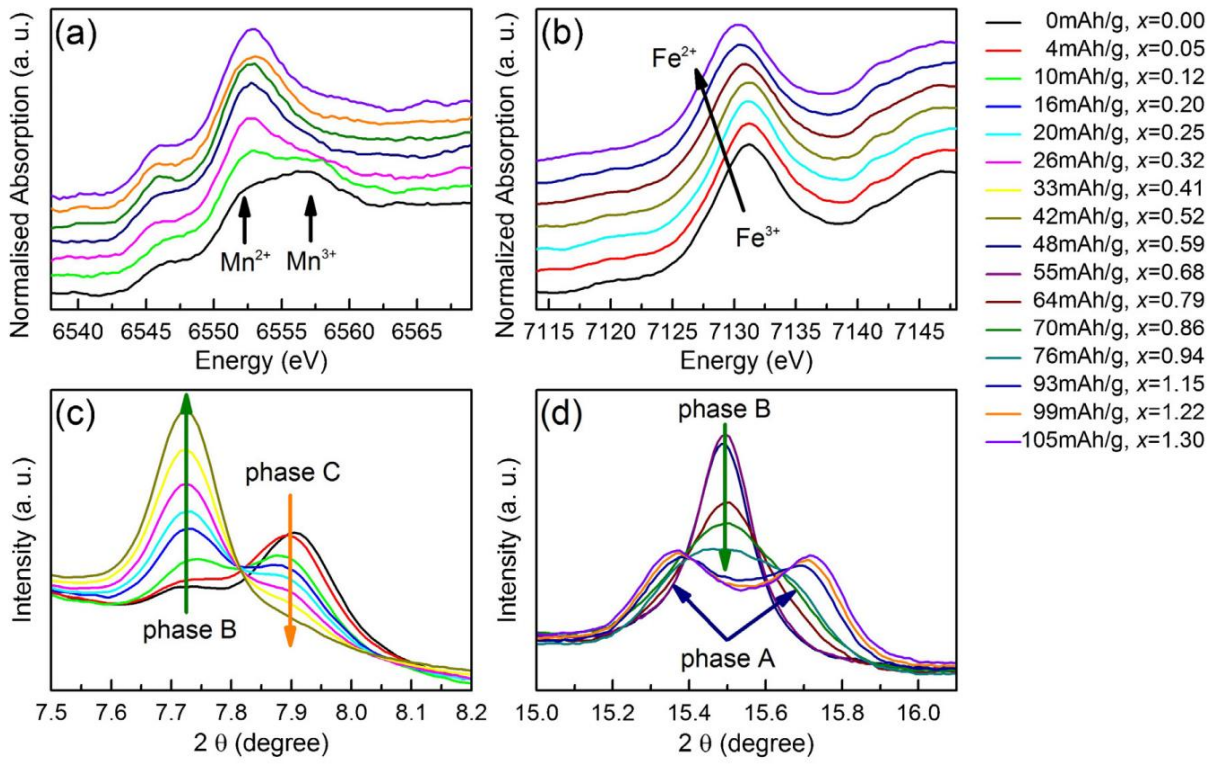

Figure 8. Changes in normalised XANES spectra and XRD profiles (λ=0.5 Å) with increasing capacity/Na content in $Na_xMn[Fe(CN)_6]_{0.83}$during discharge. XAFS signal at the Mn (a) and Fe (b) K-edges. A shift in the absorption edge position of an element to higher (lower) energies corresponds to an increase (decrease) of its average oxidation stat. c) Bragg reflections of the cubic (220) of phase C and B. d) Bragg reflections of the cubic (420) peak of phase B which splits in phase A. Relative intensities of the reflections correspond approximately to the individual phase fractions.

In essence the study shows that synthetic conditions influencing the amount of $[Fe(CN)_6]$ vacancies and the water content are critical for the performance of PBAs as battery material. With repeated cycling the active material loses Mn in the form of $NaMnCl_3$ which causes capacity degradation. Loss of capacity appears to be promoted by both, coordinating water in $[Fe(CN)_6]$ vacancies and higher zeolitic water content in the pristine material.

Another interesting development has been the object of study on the former SNB station and presented under the title: "*In situ characterization of catalysts and membranes in a microchannel under high-temperature water gas shift reaction conditions*" by Grunwaldt et al. In this study the authors investigate the use of a Microchannel Reactor (MR) for the water gas shift (WGS) reaction: $CO + H_2O \leftrightarrow CO_2 + H_2$ under operando conditions.
MR's have a high surface to volume ratio and high heat and mass transfer coefficients and have shown to have a high potential to intensify production efficiency. Membrane reactors can shift the equilibrium limitation by continuously removing one of the reaction products from the reaction area. Therefore the integration of H_2 selective membranes into MRs for hydrogen production processes was investigated.

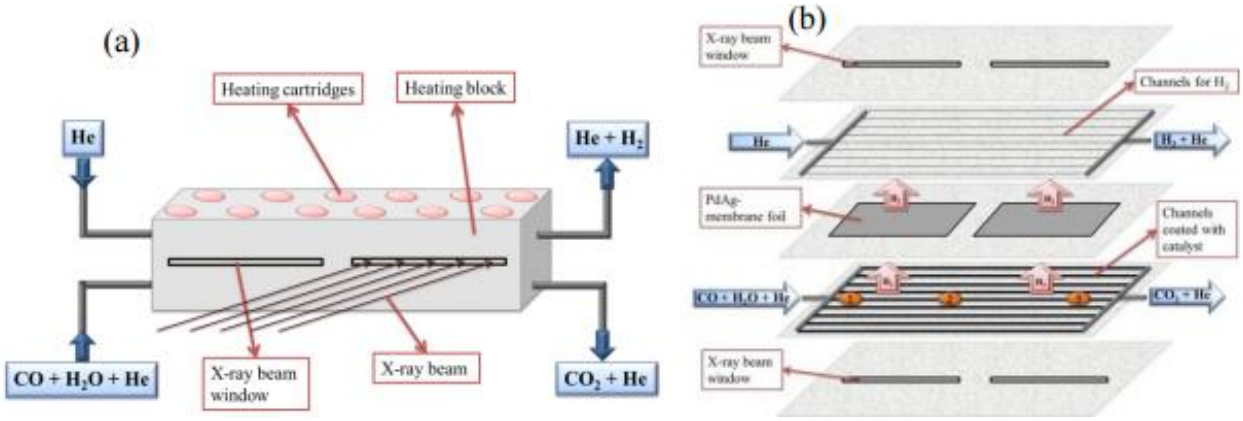

Figure 9. (a) Schematic drawing of the microreactor prototype for in situ spectroscopic studies of catalysts and membranes under WGS conditions (b) Reactor window, channel plates for reactants and the produced hydrogen, and hydrogen selective PdAg membrane foil.

The reactor showed the expected behaviour: XANES and EXAFS data (in a k-range up to 15 $Å^{-1}$) could be acquired on the Pd K-edge of the PdAg foil in the microreactor during different stages: at room temperature before the channels were coated, after coating with 10.5 wt.% Rh/CeO2 and after applying WGS reaction conditions. The reactor remained stable and gas tight at high temperature and in CO/H_2O reaction atmosphere. This new development opens up a new technique for enhancing catalytic processes allowing their study under operando conditions.

A beautiful study on water splitting done on BM01B from a group of Swiss based scientists was published in JACS under "*Promoting Photochemical Water Oxidation with Metallic Band Structures*". Photochemical water splitting is a hot topic in energy research and huge efforts are made to create systems which convert energy from sunlight directly into chemical energy (Hydrogen) by water splitting. So far, the exploration has been mainly empirical. Elucidating the correlations between electronic properties and catalytic activity is crucial for deriving catalyst design principles.

Therefore, strongly correlated electronic systems with abundant and easily tuneable electronic properties, namely $La_{1-x}Sr_xBO_3$ perovskites and $La_{2-x}Sr_xBO_4$ layered perovskites (B = Fe, Co, Ni, or Mn), were employed in this study as model systems to identify favourable electronic structures for water oxidation. It allowed establishing a direct correlation between the enhancement of catalytic activity and the insulator to metal transition by tuning the electronic properties of the target perovskite families via the La^{3+}/Sr^{2+}ratio.
In the XAFS data (see below) the maximum continuously decreases with increasing Sr content (cf. absorption intensity difference relative to LaFeO3 spectrum in Figure 10(a) (bottom)). This trend corresponds to the gradual formation of a metallic band structure with delocalized electrons and increasingly covalent Fe – O bonds

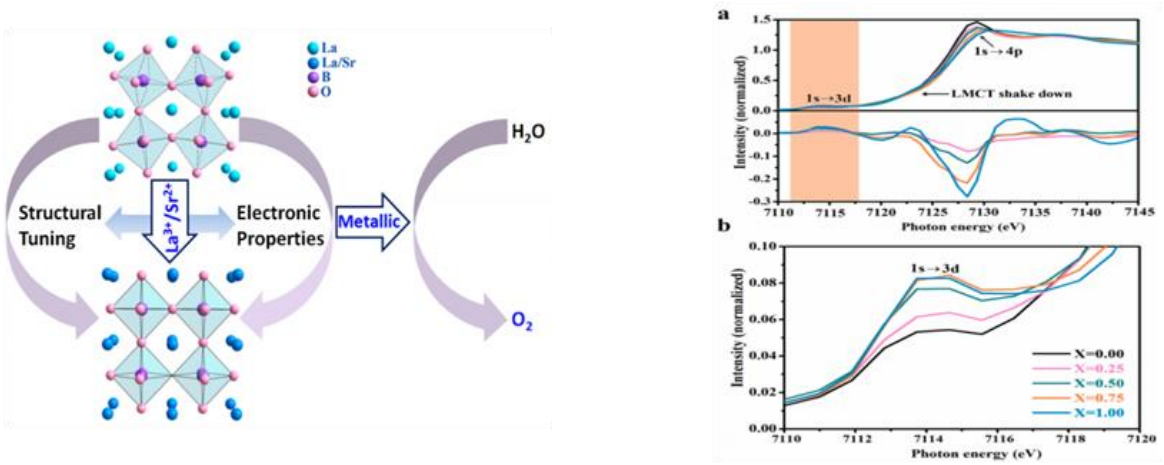

Figure 10. Left: Illustration on the tuning of the electronic properties of the target perovskite families via the La^{3+}/Sr^{2+}ratio due to an insulator to metal transition. Right: a) XAFS data of the Fe K-edge X-ray absorption spectra of $La_{1-x}Sr_xFeO_3$, and (b) zoom into the 1s to 3d transition absorption. The bottom section of (a) displays the absorption intensity difference of $La_{1-x}Sr_xFeO_3$(x = 0.25, 0.5, 0.75, 1.00) relative to $LaFeO_3$

In summary, a gradual substitution of La^{3+} by Sr^{2+} leads to an insulator to metal transition which goes hand in hand with the significant enhancement of water oxidation activity which introduces metallic properties as a promising parameter for water oxidation catalyst design.

Collaboration between SNBL and external groups

The successful Memorandum of Understanding (MoU) with the Dutch-Belgian beamline has continued to provide a mechanism for the sharing of equipment and manpower, and for the exchange of beamtime between the two CRGs. Another MoU has been in existence for several years between SNBL and MaxLab in Sweden. We have also started a collaboration with ROBL CRG (Germany) that is focused on the construction of a modified copy of PILATUS@SNBL diffractometer. Technology developed at SNBL is recognized and exported to other groups.

SNBL - FACTS AND FIGURES

BUDGET (in kEUR)

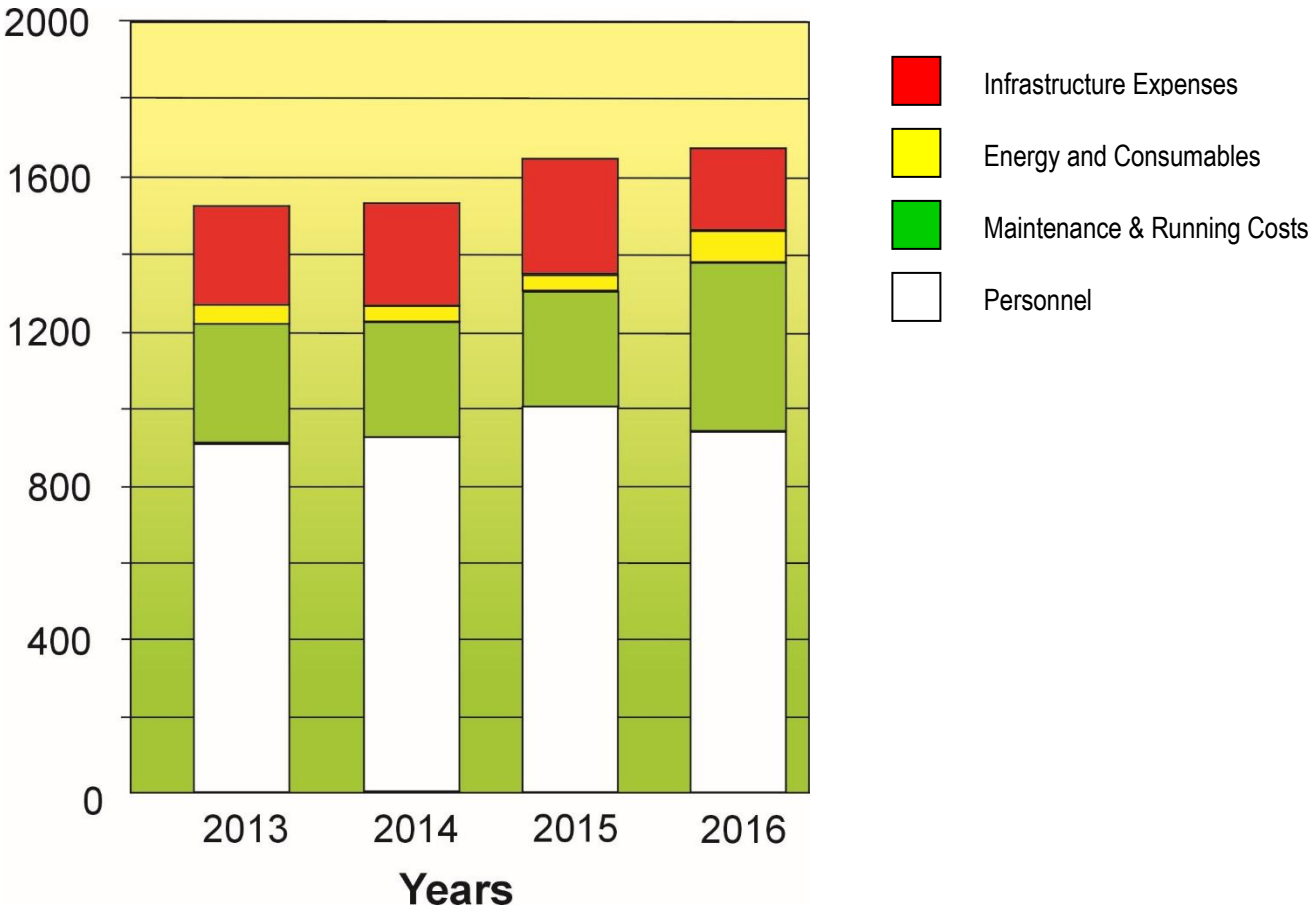

BUDGET in kCHF	2013	2014	2015	2016
Personnel	943	935	1,008	965
Maintenance and Running Costs	360	350	350	423
Energy and Consumables	47	48	48	50
Infrastructure Expenses	209	216	214	222
TOTAL	**1,540**	**1,549**	**1,620**	**1,660**

INCOME (in kEUR)

Income Outside Contract

Income According to Contract

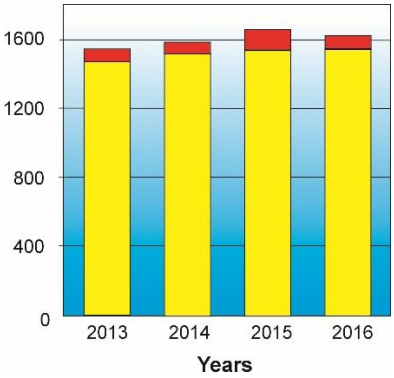

INCOME in kCHF	2013	2014	2015	2016
Income According to Contract	1,480	1,520	1,560	1,563
Income Outside Contract	58	60	59	18
Miscellaneous Income	6	13	27	35
TOTAL	**1,544**	**1,593**	**1,646**	**1,616**

EXPENDITURE (in kCHF)

Infrastructure Expenses

Energy and Consumables

Maintenance & Running Costs

Personnel

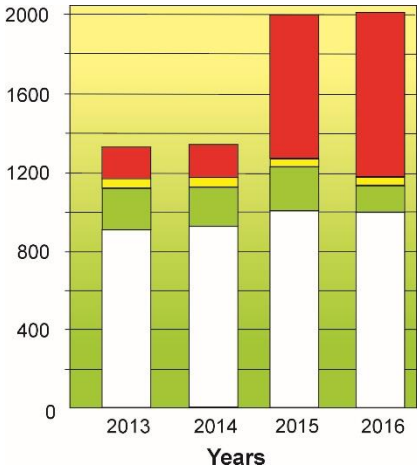

EXPENDITURE in kCHF	2013	2014	2015	2016
Personnel	954	969	1,020	1,000
Maintenance and Running Costs	180	170	189	132
Energy and Consumables	40	44	37	34
Infrastructure Expenses	147	166	166	175
BM31 Construction	-	-	590	696
TOTAL	**1,321**	**1,349**	**2,001**	**2,038**

PUBLICATIONS

Publication Rate since start-up of SNBL

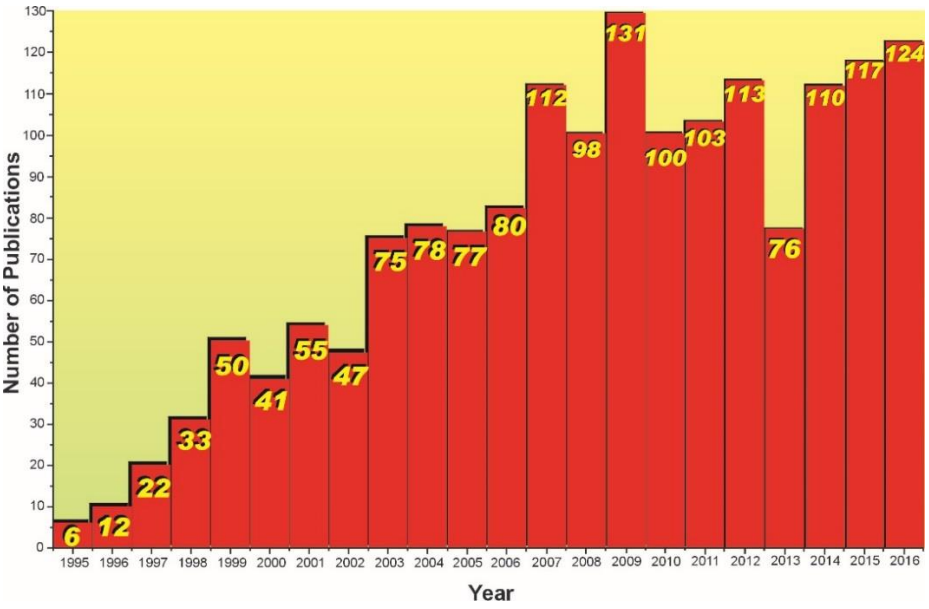

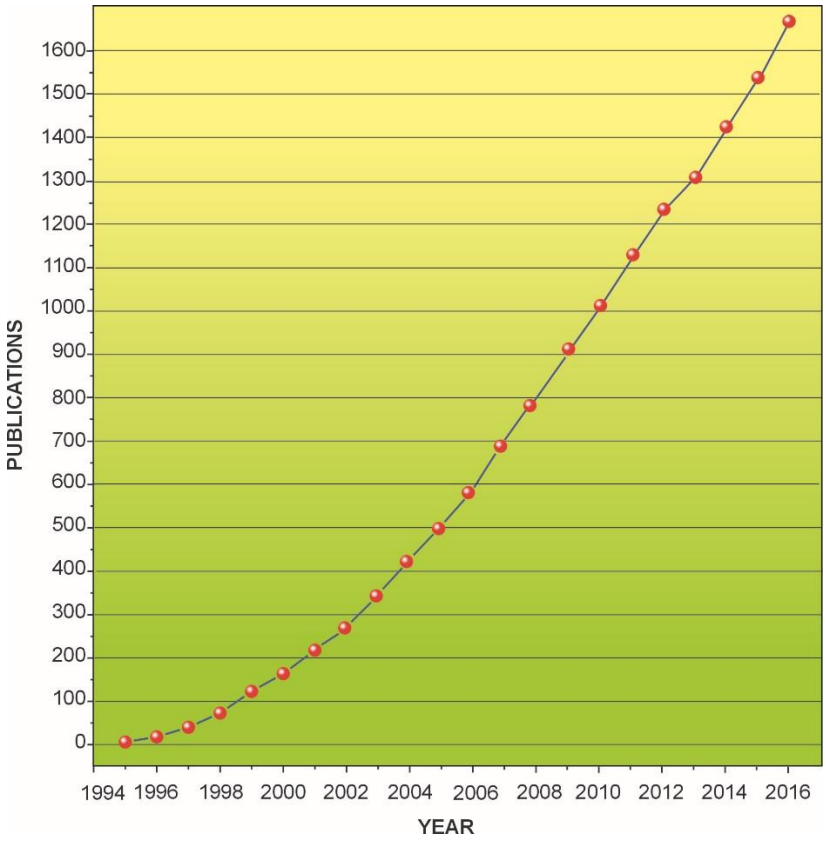

List of Publications

2015

1. **Alaimo, A.A., Takahashi, D., Cunha-Silva, L., Christou, G., Stamatatos, Th.C**. *Emissive {$Mn_4^{III}Ca$} Clusters with Square Pyramidal Topologies: Syntheses and Structural, Spectroscopic, and Physicochemical Characterization* Inorg. Chem., **54**, 5, 2137-2151, 2015
2. **Andronikova, D. A., Bosak, A. A., Bronwald, Iu. A., Burkovsky, R. G., Vakhrushev, S. B., Leontiev, N. G., Leontiev, I. N., Tagantsev, A. K., Filimonov, A. V. , Chernyshov, D. Yu.** *Critical scattering of synchrotron radiation in lead zirconate–titanate with low titanium concentrations* Physics Solid State**, 57**, 12, 2441-2446, 2015
3. **Arletti, R., Leardini, L., Vezzalini, G., Quartieri, S., Gigli, L., Santoro, M., Haines, J., Rouquette, J., Konczewicz, L.** *Pressure - induced penetration of guest molecules in high-silica zeolites: the case of mordenite* Phys. Chem. Chem. Phys., **17**, 24262-24274, 2015
4. **Bartsch, T., Niehaus, O., Johrendt, D., Kobayashi, Y., Seto, M., Abdala, P.M., Bartsch, M., Zacharias, H., Hoffmann, R.-D., Gerke, B., Rodewalda, U. Ch., Pöttgen, R**. *New quaternary arsenide oxides with square planar coordination of gold(I) – structure, ^{197}Au Mössbauer spectroscopic, XANES and XPS characterization of $Nd_{10}Au_3As_8O_{10}$ and $Sm_{10}Au_3As_8O_{10}$* Dalton Trans., **44**, 5854-5866, 2015
5. **Berthomieu, D., Gervais, Ch., Renaudin, G., Sene, S., Smith, M.E., Bonhomme, Ch., Laurencin, D.** *Coordination Polymers Based on Alkylboronate Ligands: Synthesis, Characterization, and Computational Modelling* European J. Inorganic Chemistry, **7**, 1182-1191, 2015
6. **Bleith, P., Van Beek, W., Kaiser, H., Novák, P., Villevieille, C**. *Simultaneous in Situ X-ray Absorption Spectroscopy and X-ray Diffraction Studies on Battery Materials: The Case of $Fe_{0.5}TiOPO_4$* J. Phys. Chem. C**, 119**, 7, 3466-3471, 2015
7. **Bora, D.K., Braun, A.** *Assessment of the Electronic Structure of Photo-electrodes with X-Ray and Electron Spectroscopy* From Molecules to Materials, 297-321, 2015
8. **Bosak, A., Chernyshov, D., Wehinger, B., Winkler, B., Le Tacon, M., Krisch, M.** *In-between Bragg reflections: thermal diffuse scattering and vibrational spectroscopy with x-rays In-between Bragg reflections: thermal diffuse scattering and vibrational spectroscopy with x-rays* J. Phys. D: Appl. Phys., **48**, 504003-504016, 2015
9. **Bosak, A., Krisch, M.** *Inelastic X-Ray Scattering from Phonons*, Chapter 6, X-Ray Diffraction - Modern Experimental Techniques, Pan Stanford Publishing, 145-174, 2015
10. **Boyesen, K.L., Kristiansen, T., Mathisen, K.** *Dynamic redox properties of vanadium and copper in microporous supports during the selective oxidation of propene* Catalysis Today, **254**, 21-28, 2015
11. **Brooks, L., Brunelli, M., Pattison, Ph., Jones, J.R., Fitch, A.** *Crystal structures of eight mono-methyl alkanes (C_{26}–C_{32}) via single-crystal and powder diffraction and DFT-D optimization* IUCrJ, CHEMISTRY | CRYSTENG, **2,** 5, 2052-2525, 2015
12. **Bugaev, A. L., Guda, A. A., Lomachenko, K. A., Bugaev, L. A., Soldatov, A. V**. *Pd hydride and carbide studied by means of Pd K-edge X-ray absorption near-edge structure analysis* Conference "SR-2014" Bulletin of the Russian Academy of Sciences: Physics **79**, 9, 1180-1185, 2015
13. **Bykov, M., Bykova, E., Dyadkin, V., Baumann, D., Schnick, W., Dubrovinsky, L., Dubrovinskaia, N**. *Crystal structures of cristobalite-type and coesite-type PON redetermined on the basis of single-crystal X-ray diffraction data* Acta Cryst., **E71**, 1325-1327, 2015
14. **Cai, M., Subramanian, V., Sushkevich, V.V., Ordomsky, V.V., Khodakov, A.Y**. *Effect of Sn additives on the CuZnAl–HZSM-5 hybrid catalysts for the direct DME synthesis from syngas* Applied Catalysis A: General, **502**, 370-379, 2015
15. **Cavusoglu, G., Miao, D., Lichtenberg, H., Carvalho, H.W.P., Xu, H., Goldbach, A., Grunwaldt, J.-D.** *Structure and Activity of Flame Made Ceria Supported Rh and Pt Water Gas Shift* Catalysts App. Catalysis A: General, **504**, 381-390, 2015
16. **Chaudhary, A.-L., Li, G., Matsuo, M., Orimo, Sh., Deledda, S., Sørby, M.H., Hauback, B.C., Pistidda, C., Klassen, Th., Dornheim, M.** *Simultaneous desorption behavior of M borohydrides and Mg_2FeH_6 reactive hydride composites (M = Mg, then Li, Na, K, Ca)* Appl. Phys. Lett. **107**, 073905-073909, 2015

17. **Chernyshov, D.** *Crystallography with synchrotron light* J. Phys. D: Appl. Phys. **48,** 504001-504010, 2015
18. **Chernyshov, D., Dyadkin, V., Bosak, A.** *Diffuse scattering in lead-based relaxors: synchrotron experiments, data, and models* Phase Transitions: A Multinational J., **88**, 3, 2015
19. **Danisi, R.M., Armbruster, Th., Arletti, R., Gatta, G.D., Vezzalini, G., Quartieri, S., Dmitriev, V.** *Elastic behavior and pressure-induced structural modifications of the microporous $Ca(VO)Si_4O_{10}·4H_2O$ dimorphs cavansite and pentagonite* Microp. & Mesop. Mat., **204**, 257–268, 2015
20. **Dejoie, C., Smeets, S., Baerlocher, Ch., Tamura, N., Pattison, Ph., Abela, R., McCusker, L.B.** *Serial snapshot crystallography for materials science with SwissFEL* IUCrJ, **2**, 3, 361-370, 2015
21. **Delgado, T., Tissot, A., Besnard, C., Guenee, L., Pattison, Ph., Hauser, A.** *Structural Investigation of the High Spin[RIGHTWARDS ARROW]Low Spin Relaxation Dynamics of the Porous Coordination Network $[Fe(pz)Pt(CN)_4]$-2.6 H_2O†* Chemistry - A European J., **21,** 9, 3664-3670, 2015
22. **Denys, R.V., Yartys, V.A., Gray, E.M., Webb, C.J.** *LaNi$_5$-Assisted Hydrogenation of $MgNi_2$ in the Hybrid Structures of $La_{1.09}Mg_{1.91}Ni_9D_{9.5}$ and $La_{0.91}Mg_{2.09}Ni_9D_{9.4}$* Energies, **8**, 4, 3198-3211, 2015
23. **Dmitriev V.** *Phenomenological order parameter and local parameters fluctuation far beyond the critical region of the continuous phase transition* Physica B: Condensed Matter, **472**, 97-101, 2015
24. **Dovgaliuk, I., Jepsen, L.H., Safin, D.A., £odziana, Z., Dyadkin, V., Jensen, T.R., Devillers, M., Filinchuk, Y.** *A Composite of Complex and Chemical Hydrides Yields the First Al-Based Amidoborane with Improved Hydrogen Storage Properties* Chem. - A Europ. J., **21**, 41, 14562–14570, 2015
25. **Dovgaliuk, I., Le Duff, C., Robeyns, K., Devillers, M., Filinchuk, Y.** *Mild Dehydrogenation of Ammonia Borane Complexed with Aluminium Borohydride* Chem. Mater., **27**, 3, 768-777, 2015
26. **Dyadkin, V., Mushenok, F., Bosak, A., Menzel, D., Grigoriev, S., Pattison, P., Chernyshov, D.** *Structural disorder versus chiral magnetism in $Cr_{1/3}NbS_2$* Phys. Rev. B **91**, 184205-184215, 2015
27. **Eschemann, Th. O., Lamme, W.S., Manchester, R.L., Parmentier, T.E., Cognigni, A., Rønning, M., de Jonga, K.P.** *Effect of support surface treatment on the synthesis, structure, and performance of Co/CNT Fischer–Tropsch catalysts* J. Catalysis, **328**, 130–138, 2015
28. **Evangelisti, F., Moré, R., Hodel, F., Luber, S., Patzke, G.R.** *3d–4f $\{CoII_3Ln(OR)_4\}$ Cubanes as Bio-Inspired Water Oxidation Catalysts* J. Am. Chem. Soc., **137**, 34, 11076–11084, 2015
29. **Fadaee, F., Amirnasr, M., Prša, K., Pattison, Ph., Shaik, N.E., Rønnow, H.M., Esrafili, M.D., Omrani, A.A., Amiri, A., Schenk-Joß, K.** *Intrachain antiferromagnetic exchange in a 1D branched-chain built of two different copper(II) centres interlinked by end-on azido and phenoxo bridges: electron density map, electrochemical and magnetic properties* RSC Adv., **5**, 74, 59926-59934, 2015
30. **Frommen, Ch., Heere, M., Riktor, M.B., Sorby, M.H., Hauback, B.C.** *Hydrogen storage properties of rare earth (RE) borohydrides (RE = La, Er) in composite mixtures with $LiBH_4$ and LiH* J. Alloys & Compounds, **645**, 1, S155-S159, 2015
31. **Gigli, L., Arletti, R., Vitillo, J.G., Alberto, G., Martra, G., Devaux, A., Vezzalini, G.** ***Thionine*** *Dye Confined in Zeolite L: Synthesis Location and Optical Properties* J. Phys. Chem. C, **119**, 28, 16156-16165, 2015
32. **Gremminger, A.Th., De Carvalho, H.W.P., Popescu, R., Grunwaldt, J.-D., Deutschmann. O.** *Influence of gas composition on activity and durability of bimetallic Pd-Pt/Al_2O_3 catalysts for total oxidation of methane* Catalysis Today, **258**, 2, 470-480, 2015
33. **Grzesiak, I., Ruschewitz, U.** *Crystal Structure of Cesium Phenylacetylide, $CsC_2C_6H_5$, Solved and Refined from Synchrotron Powder Diffraction Data* Z. Anorganische und allgemeine Chemie, **641**, 14, 2376-2379, 2015
34. **Guda, A. A., Pankin, I. A., Bugaev, A. L., Lomachenko, K. A., Guda, S. A., Dmitriev, V. P., Soldatov, A. V**. *X-ray absorption spectroscopy determination of the products of manganese borohydride decomposition upon heating* Bulletin Russian Academy Sciences: Physics, **79**, 1, 139-143, 2015
35. **Guzik, M.N., Deledda, S., Sørby, M.H., Yartys, V.A., Hauback, B.C.** *New FCC Mg–Zr and Mg–Zr–ti deuterides obtained by reactive milling* J. Solid State Chemistry, **226**, 237-242, 2015
36. **He, L., Li, H.W., Nakajima, H., Tumanov, N., Filinchuk, Y., Hwang, S.-J., Sharma, M., Hagemann, H., Akiba, E.** *Synthesis of a Bimetallic Dodecaborate $LiNaB_{12}H_{12}$ with Outstanding Superionic Conductivity* Chem. Mater., **27**, 16, 5483–5486, 2015

37. **He, A., Svitlyk, V., Chernyshov, D., Mozharivskyj, Y.** *Identification, structural characterization and transformations of the high-temperature $Zn_{9-\delta}Sb_7$ phase in the Zn-Sb system* Dalton Transactions, **44**, 20983-20990, 2015
38. **Hino, S., Grove, H., Ichikawa, T., Kojima, Y., Sørby, M.H., Hauback, B.C**. *Metal aluminum amides for hydrogen storage – Crystal structure studies* Int. J. Hydrogen Energy, **40,** 47, 16938-16947, 2015
39. **Hosseini, D., Imtiaz, Q., Abdala, P., Yoon, S., Kierzkoska, A., Weidenkaff, A., Müller, R.Ch.** *CuO promoted, Mn_2O_3 oxygen carriers for chemical looping based CO_2 capture* J. Mater. Chem. A, **3**, 10545-10550, 2015
40. **Humphries, T.D., Ley, M.B., Frommen, Ch., Munroe, K.T., Jensen, T.R., Hauback, B.C**. *Crystal structure and in situ decomposition of $Eu(BH_4)_2$ and $Sm(BH_4)_2$†* J. Mater. Chem. A, **3**, 691-698, 2015
41. **Humphries, T.D., Takagi, S., Li, G., Matsuo, M., Sato, T., Sørby, M.H., Deledda, S., Hauback, M.H., Orimo, Sh-i.** *Complex transition metal hydrides incorporating ionic hydrogen: Synthesis and characterization of $Na_2Mg_2FeH_8$ and $Na_2Mg_2RuH_8$* J. Alloys and Compounds, **645**, 1, S347-S352, 2015
42. **Isanov, R., Holmelid, B., Törnroos, K.W., Sydnesa, L.K.** *Synthesis of (E)-1,1-Diethoxy-3-(3-hydroxy-3-arylfuro[2,3-b]quinoxalin-2 (3H)-ylidene)propan-2-ones via Acid-Catalyzed, Stereoselective 5-Exo-Dig Cyclization* J. Heterocyclic Chem., **52**, 711, 2015
43. **Ismailova, L., Bobrov, A., Bykov, M., Bykova, E., Cerantola, V., Kantor, I., Kupenko, I., McCammon, C., Dyadkin, V., Chernyshov, D., Pascarelli, S., Chumakov, A., Dubrovinskaia, N., Dubrovinsky, L.** *High-pressure synthesis of skiagite-majorite garnet and investigation of its crystal structure* American Mineralogist , **100**, 11-12, 2650-2654, 2015
44. **Jepsen, L.H., Lee, Y.-S., Cerný, R., Sarusie, R.S., Cho, Y.W., Besenbacher, F., Jensen, T.R.** *Ammine Calcium and Strontium Borohydrides: Syntheses, Structures, and Properties* ChemSusChem, **8**, 20, 3472-3482, 2015
45. **Jepsen, L.H., Ley, M.B., Cerný, R., Lee, Y-Su., Cho, Y.W., Ravnsbæk, D., Besenbacher, F., Skibsted, J., Jensen, T.R.** *Trends in Syntheses, Structures, and Properties for Three Series of Ammine Rare-Earth Metal Borohydrides, $M(BH_4)_3{\cdot}nNH_3$ (M = Y, Gd, and Dy)* Inorg. Chem., **54**, 15, 7402–7414, 2015
46. **Jepsen, L.H., Ley, M.B., Filinchuk, Y., Besenbacher, F., Jensen, T.R.** *Tailoring the Properties of Ammine Metal Borohydrides for Solid-State Hydrogen Storage* ChemSusChem, **8**, 8, 1452-1463, 2015
47. **Khalifeh, M., Saasen, A., Vrålstad, T., Larsen, H.B., Hodne, H.** *Cap Rock Restoration in Plug and Abandonment Operations; Possible Utilization of Aplite-Based Geopolymers for Permanent Zonal Isolation and Well Plugging* SPE Offshore Europe Conference and Exhibition, Aberdeen, Scotland, UK, 2015
48. **Korzhenevskii, A L , Dmitriev, V.** *Strain induced incommensurate structures in vicinity of reconstructive phase transitions* J. Physics: Condensed Matter, **27**, 375401-375406, 2015
49. **Kränzlin, N., Van Beek, W., Niederberger, M., Koziej, D.** *Mechanistic Studies as a Tool for the Design of Copper-Based Heterostructures* Advanced Materials Interfaces, **2**, 9, 1500094-15000101, 2015
50. **Leontyev, I.N., Leontyeva, D.V., Kuriganova, A.V., Popov, Y.V., Maslova, O.A., Glebova, N.V., Nechitailov, A.A., Zelenina, N.K., Tomasov, A.A., Hennet, L., Smirnova, N.V.** *Characterization of the electrocatalytic activity of carbon-supported platinum-based catalysts by thermal gravimetric analysis* Mendeleev Commun., **25**, 468-469, 2015
51. **Le Roux, E., De Mallmann, A., Merle, N., Taoufik, M., Anwander, R.** *Immobilization of Heteroleptic Bis(oxazoline) Zinc Catalysts on SBA-15 for Asymmetric Hydrosilylation* Organometallics, **34,** 20, 5146-5154, 2015
52. **Lezcano-Gonzalez, I., Wragg, D.S., Slawinski, W.A.A., Hemelsoet, K., Van Yperen-De Deyne, A., Waroquier, M., Van Speybroeck, V., Beale, A.M.** *Determination of the Nature of the Cu Coordination Complexes Formed in the Presence of NO and NH_3 within SSZ-13* J. Phys. Chem. C, **119**, 43, 24393-24403, 2015
53. **Liu, H., Zhou, Y., Moré, R., Müller, R., Fox, Th., Patzke, G.R**. *Correlations among Structure, Electronic Properties, and Photochemical Water Oxidation: A Case Study on Lithium Cobalt Oxides* ACS Catal., **5**, 6, 3791–3800, 2015
54. **Llewellyn, Ph., Garcia-Rates, M., Gaberová, L., Miller, S.R., Devic, Th., Lavalley, J.-C., Bourrelly, S., Bloch, E., Filinchuk, Y., Wright, P.A., Serre, Ch., Vimont, A., Maurin, G.** *Structural Origin of Unusual CO_2 Adsorption Behavior of a Small-Pore Aluminum Bisphosphonate MOF* J. Phys. Chem. C, 119, 8, 4208–4216, 2015

55. **Lotti, P., Arletti, R., Gatta, G.D., Quartierie, S., Vezzalini, G., Merlini, M., Dmitriev, V., Hanfland, M.** *Compressibility and crystal-fluid interactions in all-silica ferrierite at high pressure* Microp.& Mesop. Materials, **218**, 42-54, 2015
56. **Mager, N., Robeyns,K., Hermans, S.** *Synthesis of water-soluble ruthenium clusters by reaction with PTA (1,3,5-triaza-7-phosphaadamantane)* J. Organometallic Chemistry, **794**, 48-58, 2015
57. **Maity, A., Dutta, R., Penkala, B., Ceretti, M., Letrouit-Lebranchu, A., Chernyshov, D., Perichon, A., Piovano, A., Bossak, A., Meven, M.** *Solid-state reactivity explored in situ by synchrotron radiation on single crystals: from SrFeO2.5 to SrFeO3 via electrochemical oxygen intercalation* J. Phys. D: Appl. Phys., **48**, 504004-504018, 2015
58. **Makarova, I.P.** *Superprotonics—crystals with rearranging hydrogen bonds* Physics of the Solid State, **57**, 442-449, 2015
59. **Mazzone, D. G., Gerber, S., Gavilano, J. L., Sibille, R., Medarde, M., Delley, B., Ramakrishnan, R., Neugebauer, M., Regnault, P., Chernyshov, D., Piovano, A., Fernández-Díaz, T. M., Keller, L., Cervellino, A., Pomjakushina, E., Conder, K., Kenzelmannat, M.** *Crystal structure and phonon softening in $Ca_3Ir_4Sn_{13}$* Phys. Rev. B **92**, 024101 –024111, 2015
60. **Mikheykin, A.S., Torgashev, V.I., Yuzyuk, Yu.I., Bush, A.A., Talanov, V.M., Cervellino, A , Dmitriev, V.P.** *The cooperative Jahn-Teller effect and anti-isostructural phases in Ni1-xCoxCr2O4 solid solutions: synchrotron X-ray diffraction study* J. Physics and Chemistry of Solids, **86**, 42-48, 2015
61. **Mo, F., Mathiesen, R.H., Beukes, J.A., Vu, K.M.** *Rochelle salt – a structural reinvestigation with improved tools. I. The high-temperature paraelectric phase at 308 K* IUCrJ CHEMISTRY|CRYSTENG, **2**, 1, 2015
62. **Morozov, V.A., Arakcheeva, A.V., Pattison, Ph., Meert, K.W., Smet, Ph.F., Poelman, D., Gauquelin, N., Verbeeck, J., Abakumov, A.M., Hadermann, J.** *$KEu(MoO_4)_2$: Polymorphism, Structures, and Luminescent Properties* Chem. Mater., **27**, 16, 5519–5530, 2015
63. **Mortensen, P.M., de Carvalho, H.W.P., Grunwaldt, J.-D., Jensen, P.A., Jensen, A.D.** *Activity and stability of Mo_2C/ZrO_2 as catalyst for hydrodeoxygenation of mixtures of phenol and 1-octanol* J. Catalysis, **328**, 208–215, 2015
64. **Nandi, S., Sahana, A., Mandal, S., Sengupta, A., Chatterjee, A., Safin, D.A., Babashkina, M.C., Tumanov, N.A., Filinchuk, Y., Das, D.** *Hydrazine selective dual signaling chemodosimetric probe in physiological conditions and its application in live cells* Analytica Chimica Acta, **893**, 84-90, 2015
65. **Niehaus, O. Abdala, P.M., Pöttgen, R.** *The solid solutions $CeRu_{1-x}Pd_xSn$ and $CeRh_{1-x}Pd_xSn$ – Applicability of the ICF model to determine intermediate cerium valencies by comparison with XANES data* Zeitschrift für Naturforschung B., **70**, 4, 253–264, 2015
66. **Niehaus, O., Abdala, P.M., Touzani, R.St., Fokwa, B.P.T., Pöttgen, R.** *Three structure types and intermediate cerium valence in the solid solution $CeRu_{1-x}Ni_xSn$* Solid State Sciences, **40**, 36-43, 2015
67. **Niehaus, O., Ryan, D., Flacau, R., Lemoine, P., Chernyshov, D., Svitlyk, V., Cuervo-Reyes, E. , Slabon, A., Nesper, R., Schellenberg, L., Pöttgen, R**. *Complex physical properties of EuMgSi – A complementary study by neutron powder diffraction and 151Eu Mössbauer spectroscopy* J. Mater. Chem. C, **3**, 27, 7203-7215, 2015
68. **Palin, L., Caliandro, R., Viterbo, D., Milanesio, M.** *Chemical selectivity in structure determination by time dependent analysis of in situ XRPD data: a clear view of Xe thermal behavior inside a MFI zeolite* Phys. Chem. Chem. Phys., **17**, 17480-17493, 2015
69. **Plášil, J., Hloušek, J., Kasatkin, A.V., Belakovskiy, D.I., Cejka, J., Chernyshov, D.** *Ježekite, $Na8[(UO_2)(CO_3)_3](SO_4)_2{\cdot}3H_2O$, a new uranyl mineral from Jáchymov, Czech Republic* J. Geosciences, **60**, 4, 259 - 267, 2015
70. **Polfus, J.M., Xing, W., Riktor, M., Sunding, M.F., Dahl, P.I., Hanetho, S.M., Mokkelbost, T., Larring, Y., Fontaine, M.-L.,** Bredesen, R. *Enhanced O_2 Flux of $CaTi_{0.85}Fe_{0.15}O_{3-\delta}$ Based Membranes by Mn Doping* J. Am. Ceram. Soc., **1–8,** 2015
71. **Previtera, E., Tissot, A., Johns, R.W., Hauser, A.** *Directional Energy Migration in Nanoparticles of Crystalline Metal Complexes* Advanced Materials**, 27**, 11, 1832-1836, 2015
72. **Pylypko, S., Petit, E., Yot, P.G., Salles, F., Cretin, M., Miele, Ph., Demirci, U.B.** *Key Study on the Potential of Hydrazine Bisborane for Solid- and Liquid-State Chemical Hydrogen Storage* Inorg. Chem., **54,** 9, 4574–4583, 2015
73. **Pylypko, S., Zadick, A., Chatenet, M., Miele, Ph., Cretin, M., Demirc, U.B.** *A preliminary study of sodium octahydrotriborate NaB_3H_8 as potential anodic fuel of direct liquid fuel cell* J. Power Sources, **286**, 10–17, 2015

74. **Queirós, C., Leite, A., Couto, M.G.M., Cunha-Silva, L., Barone, G. et al.** *The Influence of the Amide Linkage in the FeIII-Binding Properties of Catechol-Modified Rosamine Derivatives* Chemistry - A European J., **24**, 44, 15692-15704, 2015
75. **Quesada-Cabrera, R., Filinchuk, Y., McMillan, P.F., Nies, E., Dmitriev, V. et al.** *Exploring the pressure–temperature behaviour of crystalline and plastic crystalline phases of N-isopropylpropionamide* CrystEngComm, **17**, 2562-2568, 2015
76. **Reehuis, M., Tovar, M., Többens, D. M., Pattison, Ph., Hoser, A., Lake, B.** *Competing Jahn-Teller distortions and ferrimagnetic ordering in the geometrically frustrated system* $Ni_{1-x}Cu_xCr_2O_4$ Phys. Rev. B **91**, 024407-024419, 2015
77. **Ressnig, D., Shalom, M., Patscheider, J., More, R., Evangelisti, F., Antonietti, M., Patzke, G.** *Photochemical and Electrocatalytic Water Oxidation Activity of Cobalt Carbodiimide* J. Mater. Chem. A, **3**, 5072-5082, 2015
78. **Reiten, A., Chernyshov, D., Mathiesen, R. H.** *Nebula: reconstruction and visualization of scattering data in reciprocal space* J. Appl. Cryst., **48**, 2, 2015
79. **Renaudin, G., Mesbah, A., Dilnesa, B.Z., Francois, M., Lothenbach, B.** *Crystal Chemistry of Iron Containing Cementitious AFm Layered Hydrates* Current Inorganic Chemistry, **5**, 3, 2015
80. **Richter, B., Ravnsbaek, D.B., Tumanov, N., Filinchuk, Y., Jensen, T.R.** *Manganese Borohydride; Synthesis and Characterization* Dalton Trans., **44**, 3988-3996, 2015
81. **Rothensteiner, M., Sala, S., Bonk, A. et al.** *Ce K edge XAS of ceria-based redox materials under realistic conditions for the two-step solar thermochemical dissociation of water and/or* CO_2 Phys. Chem. Chem. Phys., **17**, 26988-26996, 2015
82. **Sadikin, Y., Brighi, M., Schouwink, P., Cerný, R.** *Superionic Conduction of Sodium and Lithium in Anion-Mixed Hydroborates* $Na_3BH_4B_{12}H_{12}$ *and* $(Li_{0.7}Na_{0.3})_3BH_4B_{12}H_{12}$ Advanced Energy Materials, **5**, 21, 2015
83. **Sadikin, Y., Stare, K., Schouwink, P., Ley, M.B., Jensen, T.R., Meden, A., Cerný, R**. *Alkali metal - yttrium Borohydrides: The link between coordination of small and large rare-earth* J. Solid State Chemistry**, 225**, 231-239, 2015
84. **Safin, D., Pialat, A., Leitch, A., Tumanov, N. et al.** *Anion-induced AgI self-assemblies with electron deficient aromatic ligands: anion–p-system interactions as a driving force for templated coordination networks* Chem. Commun., **51**, 9547-9550, 2015
85. **Safin, D.A., Tumanov, N.A., Leitch, A.A., Brusso, J.L., Filinchuk, Y., Murugesu, M.** *Elucidating the elusive crystal structure of 2,4,6-tris(2-pyrimidyl)-1,3,5-triazine* CrystEngComm, **17**, 2190-2195, 2015
86. **Safonov, V.A., Safonova, O.V., Fishgoit, L.A., Kvashnina, K., Glatzel P**. *Chemical state of phosphorus in amorphous Ni–Fe–P electroplates* Surface and Coatings Technology**, 275**, 239-244, 2015
87. **Samarasingha, P.B., Thomas, Ch.I., Fjellvåg, H.** *Investigation of Li+ insertion in columbite structured* $FeNb_2O_6$ *and rutile structured* $CrNb_2O_6$ *materials* Electrochimica Acta, **153**, 232–237, 2015
88. **Schouwink, P., Hagemann, H., Embs, J. P., D'Anna, V., Cerný, R**. *Di-hydrogen contact induced lattice instabilities and structural dynamics in complex hydride perovskites* J. Phys.: Condens. Matter, **27**, 265403-265412, 2015
89. **Schouwink, P., Morelle, F., Sadikin, Y., Filinchuk, Y., Cerný, R.** *Increasing Hydrogen Density with the Cation-Anion Pair* BH_4^--NH_4^+ *in Perovskite-Type* $NH_4Ca(BH_4)_3$ Energies, **8**, 8, 8286-8299, 2015
90. **Schouwink, P., Ramel, A., Giannini, E., Cerný, R**. *Flux-assisted single crystal growth and heteroepitaxy of perovskite-type mixed-metal borohydrides* CrystEngComm, **17**, 2682-2689, 2015
91. **Schouwink, P., Sadikin, Y, Van Beek, W., Cerný, R**. *Experimental observation of polymerization from* BH_4^- *to* $B_{12}H_{12}^{2-}$ *in mixed-anion* $A_3BH_4B_{12}H_{12}$ *(A =* Rb^+, Cs^+*)* Int. J. Hydrogen Energy, **40**, 34, 10902–10907, 2015
92. **Schuh, K., Kleist, W., Høj, M., Jensen, A.D., Beato, P., Patzke, G.R., Grunwaldt, J.-D.** *Systematic study on the influence of the morphology of* α-MoO_3 *on the selective oxidation of propylene* J. Solid State Chemistry, **228**, 42-52, 2015
93. **Schuh, K., Kleist, W., Høj, M., Trouillet, V., Beato, P., Jensen, A.D. et al.** *Bismuth Molybdate Catalysts Prepared by Mild Hydrothermal Synthesis: Influence of pH on the Selective Oxidation of Propylene* Catalysts, **5**, 3, 1554-1573, 2015
94. **Senn, A.-C., Kaegi, R., Hug, S.J. et al**. *Composition and structure of Fe(III)-precipitates formed by Fe(II) oxidation in water at near-neutral pH: Interdependent effects of phosphate, silicate and Ca* Geochimica et Cosmochimica Acta, **162**, 220-246, 2015

95. **Siegfried, S.-A., Altynbaev, E. V., Chubova, N. M., Dyadkin, V., Chernyshov, D., Moskvin, E. V., Menzel, D., Heinemann, A., Schreyer, A., Grigoriev, S. V.** *Controlling the Dzyaloshinskii-Moriya interaction to alter the chiral link between structure and magnetism for $Fe_{1-x}Co_xSi$* Phys. Rev. B **91**, 184406-184410, 2015
96. **Simmance, K., Van Beek, W., Sankar, G**. *Time resolved in situ X-ray diffraction study of crystallisation processes of large pore nanoporous aluminophosphate materials* Faraday Discuss.,**177**, 237-247, 2015
97. **Sjåstad, A.O., Andersen, N.H., Vajeeston, P. et al.** *On the Thermal Stability and Structures of Layered Double Hydroxides $Mg_{1-x}Al_x(OH)_2(NO_3)_x{\cdot}mH_2O$ (0.18?=?x?=?0.38)* European J. Inorganic Chemistry, **10**, 1775–1788, 2015
98. **Skoryunov, R.V., Soloninin, A.V., Babanova, O.A. et al**. *Nuclear Magnetic Resonance Study of Atomic Motion in Bimetallic Perovskite-Type Borohydrides $ACa(BH_4)_3$ (A = K, Rb, or Cs)* J. Phys. Chem. C, **119**, 34, 19689-19696, 2015
99. **Smith, R.L., Slawinski, W.A., Lind, A., Wragg, D.S. et al**. *Nanoporous Intergrowths: how crystal growth dictates phase composition and hierarchical structure in the CHA/AEI system* Chem. Mater., **27**, 12, 4205-4215, 2015
100. **Storm, M.M., Johnsen, R.E., Younesi, R., Norby, P**. *Capillary based Li–air batteries for in situ synchrotron X-ray powder diffraction studies* J. Mater. Chem. A, **3**, 3113-3119, 2015
101. **Suarez-Alcantara, K., Sørby, M. H., Pistidda, C., Karimi, F. et al.** *Synchrotron Diffraction Studies of Hydrogen Absorption/Desorption on CaH_2 + MgB_2 Reactive Hydride Composite Mixed With Fluorinated Compounds* J. Phys. Chem. C, **119**, 21, 11430-11437, 2015
102. **Sun, Q., Mosquera-Vazquez, S. et al.** *On the role of ligand-field states for the photophysical properties of ruthenium(II) polypyridyl complexes* Coordination Chemistry Reviews, **282–283**, 87–99, 2015
103. **Taris, A., Grosso, M., Viani, A., Brundu, M. Guida, V**. *Reaction Monitoring of Cementing Materials through Multivariate Techniques Applie d to time-resolved Synchrotron X-Ray Diffraction Data* Chemical Eng. Transactions, **43,** 895-900, 2015
104. **Trueb, P., Dejoie, C., Kobas, M., Pattison, P., Peake, D. J., Radicci, V., Sobott, B. A., Walko, D. A., Broennimann, C.** *Bunch mode specific rate corrections for PILATUS3 detectors* J. Synchrotron Radiation, **22**, 3, 2015
105. **Tumanov, N., Safin, D., Richter, B., Zbigniew, L., Jensen, T.R., Garcia, Y., Filinchuk, Y.** *Challenges in the synthetic routes to $Mn(BH_4)_2$: Insight into intermediate compounds* Dalton Trans., **44**, 6571-6580, 2015
106. **Van der Maelen, J.F., Garcia-Granda, S.** ***A*** *comparative topological study of different metal-metal and metal-ligand interactions in polynuclear organometallic clusters* AIP Conf. Proc. **1642**, 563, 2015
107. **Vergentev, T. Yu., Dyadkin, V., Chernyshov, D. Yu**. *In situ cell for X-ray single-crystal diffraction experiment at electric field* J. Surface Investigation. X-ray, Synchrotron and Neutron Techniques, 9, 3, 436-441, 2015
108. **Voss, G. J. B., Fløystad, J.B., Voronov, A., Rønning, M**. *The State of Nickel as Promotor in Cobalt Fischer–Tropsch Synthesis Catalysts* Topics in Catalysis, **58**, 14, 896-904, 2015
109. **Wang, Y., Lancelot, Ch., Lamonier, C., Richard, F., Leng, K., Sun, Y., Rives, A**. *Hierarchization of Mordenite as NiW Sulfide Catalysts Support: Towards Efficient Hydrodesulfurization* ChemCatChem, **7**, 23, 3936-3944, 2015
110. **Wang, Y., Sun, Y., Lancelot, Ch. et al.** *Effect of post treatment on the local structure of hierarchical Beta prepared by desilication and the catalytic performance in Friedel–Crafts alkylation* Microp. & Mesop. Mat., **206**, 42–51, 2015
111. **Wise, M.D., Holstein, J.J., Pattison, Ph., Besnard, C., Solari, E. et al**. *Large, heterometallic 1 coordination cages based on ditopic metallo-ligands with 3-pyridyl donor groups* Chemical Science, **6,** 1004-1010, 2015
112. **Yartys, V.A., Antonov, V.E., Chernyshov, D. et al.** *Structure and chemical bonding in $MgNi_2H_3$ from combined high resolution synchrotron and neutron diffraction studies and ab initio electronic structure calculations* Acta Materialia, **98**, 416–422, 2015
113. **Yusenko, K. V., Sottmann, J., Emerich, H., Crichton, W. A., Malavasi, L., Margadonna, S**. *Hyper-expanded interlayer separations in superconducting barium intercalates of FeSe* Chemical Communications, **51**, 7112-7115, 2015
114. **Zakharov, B., Tumanov, N., Boldyreva, E**. *ß-Alanine under pressure: towards understanding the nature of phase transitions* CrystEngComm, **17**, 2074-2079, 2015
115. **Zare, D., Suffren, Y., Guénée, L., Eliseeva, S.V. et al.** *Smaller than a nanoparticle with the design of discrete polynuclear molecular complexes displaying near-infrared to visible upconversion* Dalton Trans., **44**, 2529-2540, 2015

116. **Zavorotynska, O., Deledda, S., Vitillo, J.G., Saldan, I., Guzik, M.N. et al.** *Combined X-ray and Raman Studies on the Effect of Cobalt Additives on the Decomposition of Magnesium Borohydride* Energies, **8**, 9, 9173-9190, 2015
117. **Zavorotynska, O., Saldan, I., Hino, S., Humphries, T. D., Deledda, S., Hauback, B. C**. *Hydrogen cycling in γ-Mg(BH$_4$)$_2$ with cobalt-based additives* J. Mater. Chem. A, **3**, 6592-6602, 2015

2016

1. **Alexandropoulos, D.I., Cunha-Silva, L., Lorusso, G., Evangelisti, M., Tang, J., Stamatatos, Th.** *Dodecanuclear 3d/4f-Metal Clusters with a 'Star of David' Topology: Single-Molecule Magnetism and Magnetocaloric Properties* Chem. Commun., **52**, 1693-1696, 2016
2. **Andreeva, N. V., Pertsev, N. A., Andronikova, D. A., Filimonov, A. V., Leontiev, N. G., Leontyev, I. N., Vakhrushev, S. B**. *Domain structures and correlated out-of-plane and in-plane polarization reorientations in Pb(Zr$_{0.96}$Ti$_{0.04}$)O$_3$ single crystal via piezoresponse force microscopy* AIP Advances **6**, 095211-095216, 2016
3. **Andronikova, D., Bronwald, Y., Burkovsky, R., Chernyshev, D., Filimonov, A., Nacke, B., Ye, Z.G., Vakhrushev, S.** *Critical X-Ray Scattering in Mixed Piezoelectric Material PbZr$_{0.6}$Ti$_{0.4}$O$_3$* Solid State Phenomena, **245**, 211-216, 2016
4. **Ansermet, D., Petrovic, A.P., He, Sh., Chernyshov, D., Hoesch, M., Salloum, D., Gougeon, P., Potel, M., Boeri, L., Andersen, O.K., Panagopoulos, Ch**. *Reentrant Phase Coherence in Superconducting Nanowire Composites* ACS Nano, **10**, 515, 2016
5. **Arakcheeva, A., Chernyshov, D., Spina, M., Forró, L., Horváth, E.** *CH$_3$NH$_3$PbI$_3$: precise structural consequences of water absorption at ambient conditions* Acta Cryst**., B72**, 716, 2016
6. **Arletti, R., Gigli, l., Di Renzo, F., Quartieri S**. *Evidence for the formation of stable CO2 hydrates in zeolite Na-Y: Structural characterization by synchrotron X-ray powder diffraction* Microp. & Mesop. Mater**., 228**, 248-255, 2016
7. **Arletti, R., Ronchi, L., Quartieri, S., Vezzalini, G., Ryzhikov, A., Nouali H., Daou, T.J., Patarin, J**. *Intrusion-extrusion experiments of MgCl$_2$ aqueous solution in pure silica ferrierite: Evidence of the nature of intruded liquid by in situ high pressure synchrotron X-ray powder diffraction* Microp.& Mesop. Mat., **235**, 253–260, 2016
8. **Asanova, T., Kantor, I., Asanov, I.P., Korenev, S., Yusenko, K.V.** *Thermal decomposition of ammonium hexachloroosmate* Phys. Chem. Chem. Phys., **18**, 33134-33141, 2016
9. **Baidya, T., Bera, P., Kröcher, O., Safonova, O.V., Abdala, P., Gerke, B., Poettgen, R., Priolkar, K.R., Mandal, T.K.** *Understanding the anomalous behavior of the Vegard's law in Ce$_{1-x}$M$_x$O$_2$ (M = Sn and Ti; 0< x< = 0.5) solid solutions* Phys. Chem. Chem. Phys., **18**, 13974-13983, 2016
10. **Benoit, V., Pillai, R.S., Orsi, A., Normand, P., Jobic, E., Nouar, F., Billemont, P., Bloch, E., Bourrelly, S., Devic, Th., Wright, P.A., De Weireld, G., Serre, Ch., Maurin, G., Llewellyn, Ph.L.** *MIL-91(Ti), a small pore metal–organic framework which fulfils several criteria: an upscaled green synthesis, excellent water stability, high CO$_2$ selectivity and fast CO$_2$ transport* J. Mater. Chem. A, **4**, 1383-1389, 2016
11. **Bezrukov, A.A., Törnroos, K.W., Dietzel, P.D.C.** *Variation of Desolvation Behaviour in Two Isostructural Metal–Organic Frameworks Based on a Flexible, Racemic Bifunctional Organic Linker* Eur. J. Inorg. Chem., **27**, 4430-4439, 2016
12. **Boccato, S., Sanson, A., Kantor, I., Mathon, O., Dyadkin, V., Chernyshov, D., Carnera, A., Pascarelli, S.** *Thermal and magnetic anomalies of a-iron: an exploration by extended x-ray absorption fine structure spectroscopy and synchrotron x-ray diffraction* J. Physics: Condensed Matter, **28**, 35, 2016
13. **Boeije, M. F. J., Roy, P., Guillou, F., Yibole, H., Miao, X. F., Caron, L., Banerjee, D., Van Dijk, N. H., De Groot, R. A., Brück, E**. *Efficient Room-Temperature Cooling with Magnets* Chem. Mater., **28**, 14, 4901-4905, 2016
14. **Bolotina, N. B., Gorlova, I.G., Verin, A., Titov, A. N., Arakcheeva, A. V**. *Defect structure of TiS$_3$single crystals of the A-ZrSe$_3$ type* Crystallography Reports, **61**, 6, 923–930, 2016
15. **Bouhoute, Y., Del Rosal, I., Szeto, K. C., Merle, N., Grekov, D., De Mallmann, A., Le Roux, E., Delevoye, l., Gauvin, R. M., Maron, L., Taoufik, M.** *Modification of silica-supported tungsten neosilyl oxo precatalysts: impact of substituted phenol on activity and stability in olefin metathesis* Catal. Sci. Technol., **6**, 8532-8539, 2016
16. **Bouhoute, Y., Grekov, D., Szeto, K.Ch., Merle, N., De Mallmann, A., Lefebvre, F., Raffa, G., Del Rosal, I., Maron, L., Gauvin, R.M., Delevoye, L., Taoufik, M.** *Accessing realistic models for the*

WO_3-SiO_2 industrial catalyst through the design of organometallic precursors ACS Catal., **6**, 1-18, 2016

17. **Brighi, M., Schouwink, P., Sadikin, Y., Cerny, R.** *Fast ion conduction in garnet-type metal borohydrides Li_3 K_3 $Ce_2(BH_4)12$ and Li_3 K_3 $La_2(BH_4)12$* J. Alloys & Compounds, **662**, 388-395, 2016
18. **Bronwald, I., Andronikova, D., Burkovsky, R., Chernyshev, D., Leontiev, N. G., Leontiev, I. N., Ye, Z.-G., Vakhrushev, S.** *Composition dependence of the diffuse scattering in cubic $PbZr_{1-x}Ti_xO_3$* Ferroelectrics, **503**, 1, 45-51, 2016
19. **Brunet, G., Safin, D.A., Korobkov, I., Cognigni, A., Murugesu, M.** *The Hidden Transformations of a Crystalline Sponge: Elucidating the Stability of a Highly Porous Three-Dimensional MOF* Cryst. Growth Des., **16**, 7, 4043-4050, 2016
20. **Bugaev, A L, Guda, A A ., Lomachenko, K A., Lazzarini, A., Srabionyan, V.V., Vitillo, J.G., Piovano, A., Groppo, E., Bugaev, L.A., Soldatov, A.V.** *Hydride phase formation in carbon supported palladium hydride nanoparticles by in situ EXAFS and XRD* J. Physics: Conference Series, **712**, 1, 2016
21. **Bugaev, A.L., Guda, A.A., Lomachenko, K.A., Lazzarini, A., Srabionyan, V., Vitillo, J G., Piovano, A., Groppo, E., Bugaev, L A , Soldatov, A.V., Dmitriev, V.P., Pellegrini, R., Van Bokhoven, J A ., Lamberti, C.** Hydride phase formation in carbon supported palladium hydride nanoparticles by in situ EXAFS and XRD J. Physics: Conference Series, **712**, 1, 2016
22. **Cavusoglu, G., Dallmann, F., Lichtenberg, H., Goldbach, A., Dittmeyer, R., Grunwaldt, J-D.** *In situ characterization of catalysts and membranes in a microchannel under high-temperature water gas shift reaction conditions* J. Physics: Conference Series, **712**, 1, 2016
23. **Cavusoglu, G., Lichtenberg, H., Gaur, A., Goldbach, A., Grunwaldt, J-D**. *Flame made ceria supported noble metal catalysts for efficient H_2 production via the water gas shift reaction* J. Physics: Conference Series, **712**, 1, 2016
24. **Chumakov, A.I., Monaco, G., Han, X., Xi, L., Bosak, A., Paolasini, L., Chernyshov, D., Dyadkin, V.** *Relation between the boson peak in glasses and van Hove singularity in crystals* Philosophical Magazine, **96**, 7-9, 743-753, 2016
25. **Crivello, J.-C., Denys, R. V., Dornheim, M., Felderhoff, M., Grant, D. M., Huot, J., Jensen, T. R., De Jongh, P., Latroche, M., Walker, G. S., Webb, C. J. , Yartys, V. A.** *Mg-based compounds for hydrogen and energy storage* Applied Physics A, **85,** 122-139, 2016
26. **Conterosito, E., Benesperi, I., Toson, V., Saccone, D., Barbero, N., Palin, L., Barolo, C., Gianotti, V., Milanesio, M.** *High-Throughput Preparation of New Photoactive Nanocomposites* ChemSusChem, **9,** 11, 1279-1289, 2016
27. **Dähn, R., Arakcheeva, A., Schaub, Ph., Pattison, P., Chapuis, G., Grolimund, D., Wieland, E., Leemann. A.** *Application of micro X-ray diffraction to investigate the reaction products formed by the alkali–silica reaction in concrete structures* Cement and Concrete Research, **79**, 49-56, 2016
28. **Del Campo, P., Slawinski, W.A., Henry, R., Erichsen, M.W., Svelle, S., Beato, P., Wragg, D., Olsbye, U.** *Time- and space-resolved high energy operando X-ray diffraction for monitoring the methanol to hydrocarbon reaction over H-ZSM-22 zeolite catalyst in different conditions* Surface Science**, 648**, 141-149, 2016
29. **Dharanipragada, N.V.R.A., Meledina, M., Galvita, V.V., Poelman, H., Turner, S., Van Tendeloo, G., Detavernier, Ch., Marin, G.V.** *Deactivation study of Fe_2O_3-CeO_2 during redox cycles for CO production from CO_2* Ind. Eng. Chem. Res., **55**, 20, 5911-5922, 2016
30. **Doblas, D., Rosenthal, M., Burghammer, M., Chernyshov, D., Spitzer, D., Ivanov, D.A.** *Smart Energetic Nano-Sized Co-Crystals: Exploring Fast Structure Formation and Decomposition Processes* Cryst. Growth Des., **16**, 432-439, 2016
31. **Domingos, S., Fernandes, A., Duarte, M.T., Da Piedade, M.F.M.** *New multicomponent Sulfadimethoxine Crystal forms: SULFONAMIDES as participant in supermolecular interactions* Cryst. Growth Des., **16**, 4, 1879-1892, 2016
32. **Dovgaliuk, I., Filinchuk, Y.** *Aluminium complexes of B- and N-based hydrides: Synthesis, structures and hydrogen storage properties* Int. J. Hydrogen Energy, **41**, 34, 15489-15504, 2016
33. **Dyadkin, V., Pattison, Ph., Dmitriev, V., Chernyshov, D.** *A new multipurpose diffractometer PILATUS@SNBL* J. Synchrotron Rad., **23**, 3, 2016
34. **Dyadkin, V., Wright, J., Pattison, P., Chernyshov, D.** *Probing structural chirality with high-energy synchrotron radiation* J. Applied Crystallography, **49**, 3, 2016
35. **Eymann, L.Y.M., Tskhovrebov, A.G., Sienkiewicz, A., Bila, J.L., Živkovic, I., Rønnow, H.M., Wodrich, M.D., Vannay, L., Corminboeuf, C., Pattison, Ph., Solari, E., Scopelliti, R., Severin, K.** *Neutral Aminyl Radicals Derived from Azoimidazolium Dyes* J. Am. Chem. Soc., **138**, 46, 15126-15129, 2016

36. **Gebremariam, K.F., Kvittingen, L., Nicholson, D.G.** *Multi-analytical investigation into painting materials and techniques: the wall paintings of Abuna Yemata Guh church Multi-analytical investigation into painting materials and techniques: the wall paintings of Abuna Yemata Guh church* Heritage Science, **4**, 32, 2016
37. **GharibDoust, S.P., Heere, M., Sorby, M.H., Ley, M.B., Ravnsbak, D.B., Hauback, B.C., Èernýe, R., Jensen, T.R.** *Synthesis, structure and properties of new bimetallic sodium and potassium lanthanum borohydrides†* Dalton Trans., **45**, 19002-19011, 2016
38. **Gholivand, K., Kahnouji, M., Latifi, R., Fadaei, F.T., Gholami, A., Schenk, K.J.** *Synthesis, Structure, and Catalytic Properties of Palladium Complexes Containing bis(phosphino)-amine ligands* Inorganica Chimica Acta, **448**, 61-69, 2016
39. **Grekov, G., Bouhoute, Y., Szeto, K. C., Merle, N., De Mallmann, A., Lefebvre, F., Lucas, C., Del Rosal, I.D., Maron, L., Gauvin, R.M., Delevoye, L., Taoufik, M.** *Silica-Supported Tungsten Neosilyl Oxo Precatalysts: Impact of the Podality on Activity and Stability in Olefin Metathesis* Organometallics, **35**, 13, 2188–2196, 2016
40. **Grube, E., Olesen, C.H., Ravnsbæk, D., Jensen, T.R.** *Barium borohydride chlorides; Synthesis, crystal structures and thermal properties* Dalton Trans., **45**, 19, 8291-8299, 2016
41. **Hammersley, A. P.** *FIT2D: a multi-purpose data reduction, analysis and visualization program* J. Appl. Cryst., **49**, 2016
42. **Heinz, M., Srabionyan, V.V., Bugaev, A.L., Pryadchenko, V.V., Ishenko, E.V., Avakyan, L.A., Zubavichus, Y.V. , Ihlemann, J., Meinertz, J., Pippel, E., Dubiel, M., Bugaev, L.A.** *Formation of silver nanoparticles in silicate glass using excimer laser radiation: Structural characterization by HRTEM, XRD, EXAFS and optical absorption spectra* J. Alloys and Compounds, **681**, 5, 305-315, 2016
43. **Heere, M., Payandeh GharibDoust, S.H., Frommen, Ch., Humphries, T.D., Ley, M.B., Sørby, M.H., Jensen, T.R., Hauback, B.C.** *The influence of LiH on the rehydrogenation behavior of halide free rare earth (RE) borohydrides (RE = Pr, Er)* Phys. Chem. Chem. Phys., **18**, 24387-24395, 2016
44. **Heere, M., Sørby, M.H., Pistidda, C., Dornheim, M., Hauback, B.C**. *Milling time effect of Reactive Hydride Composites of NaF-NaH-MgB_2 investigated by in situ powder diffraction* Int. J. Hydrogen Energy, **41**, 30, 13101-13108, 2016
45. **Hino, S., Ichikawa, T., Kojima, Y., Sørby, M.H., Hauback, B.C.** *A new complex alkali metal aluminium amide borohydride, $Li_2Al(ND_2)_4BH_4$: synthesis, thermal analysis and crystal structure* RSC Adv., **6**, 28761-28766, 2016
46. **Hyakutake, T., Van Beek, W., Urakawa, A.** *Unravelling the nature, evolution and spatial gradients of active species and active sites in the catalyst bed of unpromoted and K/Ba-promoted Cu/Al2O3 during CO2 capture-reduction* J. Mater. Chem. A, **4**, 6878-6885, 2016
47. **Ibsen, C.J.S., Chernyshov, D., Birkedal, H.** *Apatite Formation from Amorphous Calcium Phosphate and Mixed Amorphous Calcium Phosphate/Amorphous Calcium Carbonate* Chem. Eur. J., **22**, 1–12, 2016
48. **Imtiaz,Q., Abdala, P., Kierzkoska, A., Van Beek, W., Schweiger, S., Rupp, J.L.M., Müller, Ch.R.** *Na+ doping induced changes in the reduction and charge transport characteristics of Al2O3-stabilized, CuO-based materials for CO2 capture* Phys. Chem. Chem. Phys., **18**, 12278-12288, 2016
49. **Imtiaz,Q., Yüzbasi, N. S., Abdala, P., Kierzkowska, A. M., Van Beek, W., Broda, M., Müller, C.R**. *Development of $MgAl_2O_4$-stabilized, Cu-doped, Fe_2O_3-based oxygen carriers for thermochemical water-splitting*
J. Mater. Chem. A, **4**, 113-123, 2016
50. **Jansze, S.M., Cecot, G., Wise, M.D., Zhurov, K.O., Ronson, T.K., Castilla, A.M., Finelli, A., Pattison, Ph., Solari, E., Scopelliti, R., Zelinskii, G.E., Vologzhanina, A.V., Voloshin, Y.Z., Nitschke, J.R., Severin, K.** *Ligand Aspect Ratio as a Decisive Factor for the Self-Assembly of Coordination Cages* J. Am. Chem. Soc., **138**, 6, 2046-2054, 2016
51. **Jepsen, L., Wang, P., Wu, G., Xiong, Z., Besenbacher, F., Chen, P., Jensen, T.R.** *Synthesis and decomposition of Li3Na(NH2)4 and investigations of Li–Na–N–H based systems for hydrogen storage* Phys. Chem. Chem. Phys., **18**, 1735-1742, 2016
52. **Jepsen, L., Wang, P., Wu, G., Xiong, Z., Besenbacher, F., Chen, P., Jensen, T.R.** *Thermal decomposition of sodium amide, NaNH2, and sodium amide hydroxide composites, NaNH2-NaOH* Phys. Chem. Chem. Phys., **18**, 25257-25264, 2016
53. **Khalifeh, M., Saasen, A., Vrålstad, T., Larsen, H.B., Hodne, H.** *Experimental study on the synthesis and characterization of aplite rock-based geopolymers* J. Sustainable Cement-Based Materials, **5**, 4, 233-246, 2016

54. **Larsen, H.B., Thorkildsen, G., Nicholson, D.G., Pattison, Ph.** *Thermal induced structural properties of silver(I) sulphate (Ag_2SO_4)* Crystal Research and Technology, in press, 2016
55. **Lee, Y.-S., Ley, M.B., Jensen, T.R., Cho, Y.W.** *Lithium Ion Disorder and Conduction Mechanism in $LiCe(BH_4)_3Cl$* J. Phys. Chem. C, **120**, 34, 19035-19042, 2016
56. **Ley, M.B., Jørgensen, M., Cerný, R., Filinchuk, Y., Jensen, T.R.** *From $M(BH_4)_3$ (M = La, Ce) Borohydride Frameworks to Controllable Synthesis of Porous Hydrides and Ion Conductors* Inorg. Chem., **55**, 19, 9748-9756, 2016
57. **Liu, H., Moré, R., Grundmann, H., Cui, C., Erni, R., Patzke, G.R.** *Promoting Photochemical Water Oxidation with Metallic Band Structures* J. Am. Chem. Soc., **138**, 5, 1527–1535, 2016
58. **Luisie, N., Bally, K., Scopelliti, R., Fadaei, F.T., Schenk, K., Pattison, Ph., Solari, E., Severin, K.** *Crystal Engineering of Polymeric Structures with Dative Boron–Nitrogen Bonds: Design Criteria and Limitations* Cryst. Growth Des., **16**, 11, 6600-6604, 2016
59. **Lundvall, F., Vajeeston, P., Wragg, D.S., Dietzel, P.D.C., Fjellvåg, H.** *Two new series of Coordination Polymers and evaluation of their properties by DFT* Cryst. Growth Des., **16**, 339-346, 2015
60. **Lundvall, F., Wragg, D. S., Dietzel, P. D. C., Fjellvåg, H.** *Two new Cu(II) and La(III) 2D coordination polymers, synthesis and in situ structural analysis by X-ray diffraction* Dalton Trans., **45**, 12827-12834, 2016
61. **Maiti, S., Steurer, W.** *Structural-disorder and its effect on mechanical properties in single-phase TaNbHfZr high-entropy alloy* Acta Materialia, **106**, 87–97, 2016
62. **Makarova, I. P., Grebenev, V. V., Dmitricheva, E. V., Vasiliev, I., Komornikov, V., Dolbinina, V.V., Mikheykin, A.** *$M_mH_n(XO_4)_{(m+n)/2}$ crystals: structure, phase transitions, hydrogen bonds, conductivity. II. Structure and properties of $Cs_3(HSO_4)_2(H_2PO_4)$ and $Cs_4(HSO_4)_3(H_2PO_4)$ single crystals* Acta Cryst., **B72**, 133-141, 2016
63. **Makarova, I. P., Grebenev, V. V., Vasil'ev, I. I., Dmitricheva, E. V., Komornikov, V. A., Dolbinina, V. V., Mikheikin A.S.** *Structure of $Cs_4(HSO_4)_3(H_2PO_4)$ single crystals* Crystallography Reports, **61**, 1, 18-23, 2016
64. **Marmier, M., Cecot, G., Curchod, B.F.E., Pattison, P., Solari, E., Scopelliti, R., Severin, K**. *Surface functionalization of dinuclear clathrochelates via Pd-catalyzed cross-coupling reactions: facile synthesis of polypyridyl metalloligands* Dalton Trans., **45**, 8422-8427, 2016
65. **Marmier, M., Cecot, G., Vologzhanina, A.V., Bila, J.L., Zivkovic, I., Ronnow, H.M., Nafradi, B., Solari, E., Pattison, Ph., Scopellitia, R., Severin, K.** *Dinuclear clathrochelate complexes with pendent cyano groups as metalloligands* Dalton Trans., **45**, 15507-15516, 2016
66. **Marmier, M., Wise, M.D., Holstein, J.J., Pattison, Ph., Schenk, K., Solari, E., Scopelliti, R., Severin, K.** *Carboxylic Acid Functionalized Clathrochelate Complexes: Large, Robust, and Easy-to-Access Metalloligands* Inorg. Chem., **55**, 8, 4006-4015, 2016
67. **Mercier, G.M., Robeyns, K., Leyssens, T.** *Altering the photochromic properties of N-Salicylideneanilines using a co-crystal engineering approach* Cryst. Growth Des., **16**, 6, 3198-3205, 2016
68. **Møller, K.T., Ley, M.B., Schouwink, P., Cerný, R., Jensen, T.R.** *Synthesis and thermal stability of perovskite alkali metal strontium borohydrides* Dalton Trans., **45**, 831-840, 2016
69. **Monchak, M., Hupfer, Th., Senyshyn, A., Boysen, H., Chernyshov, D., Hansen, Th., Schell, K.G., Bucharsky, E.C., Hoffmann, M.J., Ehrenberg, H**. *Lithium Diffusion Pathway in $Li_{1.3}Al_{0.3}Ti_{1.7}(PO_4)_3$ (LATP) Superionic Conductor* Inorg. Chem., **55**, 6, 2941-2945, 2016
70. **Morelle, F., Jepsen, L.H., Jensen, T.R., Sharma, M., Hagemann, H., Filinchuk, Y.** *Reaction Pathways in $Ca(BH_4)_2$-$NaNH_2$ and $Mg(BH_4)_2$-$NaNH_2$ Hydrogen-rich* Systems J. Phys. Chem. C, **120**, 16, 8428-8435, 2016
71. **Moury, R., Robeyns, K., Filinchuk, Y., Miele, Ph., Demirci, U.B.** *In situ thermodiffraction to monitor synthesis and thermolysis of hydrazine borane-based materials* J. Alloys & Compounds, **659**, 210-216, 2016
72. **Náfrádi, B., Szirmai, P., Spina, M., Lee, H., Yazyev, O. V., Arakcheeva, A., Chernyshov, D., Gibert, M., Forró, F., Horváth, E**. *Optically switched magnetism in photovoltaic perovskite $CH_3NH_3(Mn:Pb)I_3$* Nature Communications, **7**, 13406, 2016
73. **Nakagawa, T., Yuan, Z., Zhang, J., Yusenko, K.V., Drathen, Ch., Liu, Q., Margadonna, S., Jin, C**. *Structure and magnetic property of potassium intercalated pentacene: observation of superconducting phase in $K_x C_{22}H_{14}$* J. Physics: Condensed Matter, **28**, 48, 484001- 484009, 2016
74. **Newton, M.A., Brazier, J.B., Barreiro, E.M., Emerich, H., Adrio, L.A., Mulligan, Ch.J., Hellgardtd, K., Hii, K.K**. *Restructuring of supported Pd by green solvents: an operando quick EXAFS (QEXAFS) study and implications for the derivation of structure–function relationships in Pd catalysis* Catal. Sci. Technol., **6**, 8525-8531, 2016

75. **Newton, M.A., Brazier, J.B., Barreiro, E.M., Parry, S., Emerich, H., Adrio, L.A., Mulligan, Ch.J., Hellgardt, K., Kuok (Mimi) Hii, K.** *Operando XAFS of supported Pd nanoparticles in flowing ethanol/water mixtures: implications for catalysis* Green Chem., 18, 406-411, 2016
76. **Ovsyannikov, S.V., Bykov, M., Bykova, E., Kozlenko, D.P., Tsirlin, A.A., Karkin, A.E., Shchennikov, V.V., Kichanov, S.E., Gou, H., Abakumov, A.M., Egoavil, R., Verbeeck, J., McCammon, C., Dyadkin, V., Chernyshov, D., Van Smaalen, S., Dubrovinsky, L.S.** *Charge-ordering transition in iron oxide Fe_4O_5 involving competing dimer and trimer formation* Nature Chemistry, **8**, 501-508, 2016
77. **Øygarden, V., Fjellvåg, H., Sørby, M.H., Sjåstad, A.O.** *Crystal Structure of $LaSr_3Fe_3O_8(OH)_2{\cdot}xH_2O$* Inorg. Chem., **55**, 15, 7630-7636, 2016
78. **Palin, L., Conterosito, E., Caliandro, R., Boccaleri, E., Croce, G., Kumar, S., Van Beek, W., Milanesio, M.** *Rational design of the solid-state synthesis of materials based on poly-aromatic molecular complexes* CrystEngComm, **18**, 5930-5939, 2016
79. **Petrovic, A. P., Ansermet, D., Chernyshov, D., Hoesch, M., Salloum, D., Gougeon, P., Potel, M., Boeri, L., Panagopoulos, C**. *A disorder-enhanced quasi-one-dimensional superconductor* Nature Communications, **7**, N 12262
80. **Picasso, C.V., Safina, D.A., Dovgaliuk, I., Devred, F., Debecker, D., Li, H.-W., Proost, J., Filinchuk, Y.** *Reduction of CO_2 with KBH4 in solvent-free conditions* Int. J. Hydrogen Energy, **41**, 32, 14377-14386, 2016
81. **Pohl, A., Faraz, M., Schröder, A., Baunach, M., Schabel, W., Guda, A., Shapovalov, V., Soldatov, A., Chakravadhanula, V., Kübel, Ch., Witte,R., Hahn, H., Diemant, Th., Behm R.J., Emerich, H., Fichtner, M.** *Development of a water based process for stable conversion cathodes on the basis of FeF_3* J. Power Sources, **313**, 213–222, 2016
82. **Polfus,J.M., Fontaine, M.-L., Thøgersen, A., Riktor, M., Norby, T., Bredesen, R.** *Solubility of transition metal interstitials in proton conducting $BaZrO_3$ and similar perovskite oxides* J. Mater. Chem. A, **4**, 8105-8112, 2016
83. **Polfus, J.M., Xing, W., Riktor, M., Sunding, M.F., Dahl, P.I., Hanetho, S.M., Mokkelbost, T., Larring, Y., Fontaine, M.-L., Bredesen, R**. *Enhanced O_2 Flux of $CaTi_{0.85}Fe_{0.15}O_{3-d}$ Based Membranes by Mn Doping* J. Am. Ceram. Soc., **99**, 3, 1071–1078, 2016
84. **Razumnaya, A.G., Mikheykin, A.S., Lukyanchuk, I.A., Shirokov, V.V., Golovko, Y.I., Mukhortov, V.M., Marssi, M.L., Yuzyuk, Y.I.** *Unexpectedly high Curie temperature in weakly strained ferroelectric film* Phys. Status Solidi **B**, 1–6, 2016
85. **Reehuis, M., Ulrich, C., Abdala, P. M., Pattison, P., Khaliullin, G., Fujioka, J., Miyasaka, S., Tokura, Y., Keimer, B**. *Spin and orbital disordering by hole doping in $Pr_{1-x}Ca_xVO_3$* Phys. Rev. B **94**, 10, 104436-10444, 2016
86. **Ribeiro, M.A., Stasiw, D.E., Pattison, Ph., Raithby, P.R., Shultz, D.A., Pinheiro, C.B.** *Towards Controlling the Solid State Valence Tautomeric Interconversion Character by Solvation* Cryst. Growth Des., **16**, 4, 2385-2393, 2016
87. **Rothensteiner, M., Bonk, A., Vogt, U.F., Emerich, H., Van Bokhoven, J.A.** *Structural Changes in Ce0.5Zr0.5O2-d under Temperature-swing and Isothermal Solar Thermochemical Looping Conditions Determined by in situ Ce K and Zr K Edge XAS* J. Phys. Chem. C, **120**, 26, 13931-13941, 2016
88. **Safin, D.A., Babashkina, M.G., Mitoraj, M.P., Kubisiak, P., Robeyns, K., Boltec, M., Garcia, Y**. *An intermolecular pyrene excimer in the pyrene-labeled N-thiophosphorylated thiourea and its nickel(II) complex* Inorg. Chem. Front., **3**, 1419-1431, 2016
89. **Samarasingha, P.B., Sottmann, J., Margadonna, S., Emerich, H., Nilsen, O., Fjellvåg, H.** *In situ synchrotron study of ordered and disordered $LiMn_{1.5}Ni_{0.5}O_4$ as lithium ion battery positive electrode* Acta Materialia, **116**, 290–297, 2016
90. **Sandbrink, L., Klindtworth, E., Islam, H.-U., Beale, A.M., Palkovits, R.** *ReO_x/TiO_2: A Recyclable Solid Catalyst for Deoxydehydration* ACS Catal., **6**, 677–680, 2016
91. **Sato, T., Takagi, S., Deledda, S., Hauback, B.S., Orimo, Sh.-i.** *Extending the applicability of the Goldschmidt tolerance factor to arbitrary ionic compounds* Scientific Reports, **6**, 23592, 2016
92. **Schouwink, P., Didelot, E., Lee, Y.-S., Mazet, Th., Cerný, R**. *Structural and magnetocaloric properties of novel gadolinium borohydrides* J. Alloys & Compounds, **664**, 378–384, 2016
93. **Sharma, M., Didelot, E., Spyratou, A., Daku, L.M.L., Cerný, R., Hagemann, H.** *Halide Free $M(BH_4)_2$ (M = Sr, Ba, and Eu) Synthesis, Structure, and Decomposition* Inorg. Chem., **55**, 14, 7090–7097, 2016
94. **Sikolenko, V V., Troyanchuk, I O., Efimov, V V., Efimova, E A., Tiutiunnikov, S I., Karpinsky, D V., Pascarelli, S., Zaharko, O., Ignatov, A. Aquilanti, D., Selutin, A G., Shmakov, A N.,**

Prabhakaran, D. *EXAFS and X-ray diffraction study of $LaCoO_3$ across the spin-state transition* J. Physics: Conference Series, **712**, 1, 2016

95. **Slawinski, W. A., Fjellvåg, Ø.S., Ruud, A., Fjellvåg, H**. *A novel polytype - the stacking fault based γ-MoO_3 nanobelts* Acta Cryst., **B72**, 201-208, 2016
96. **Slawinski, W. A., Sjåstad, A.O., Fjellvåg, H.** *Stacking Faults and Polytypes for Layered Double Hydroxides: What Can We Learn from Simulated and Experimental X-ray Powder Diffraction Data?* Inorg. Chem., **55**, 24, 12881–12889, 2016
97. **Sottmann, J., Bernal, F.L.M., Yusenko, K.V., Herrmann, M., Emerich, H., Wragg, D.S., Margadonna, S.** *In operando Synchrotron XRD/XAS Investigation of Sodium Insertion into the Prussian Blue Analogue Cathode Material $Na_{1.32}Mn[Fe(CN)_6]_{0.83}$·z H_2O* Electrochimica Acta, **200**, 305-313, 2016
98. **Sottmann, J., Herrmann, M., Vajeeston, P., Hu, Y., Ruud, A., Drathen, Ch., Emerich, H., Fjellvåg, H., Wragg, D.S.** *How Crystallite Size Controls Reaction Path in Non-Aqueous Metal Ion Batteries: The Example of Sodium Bismuth Alloying.* Chem. Mater., **28**, 8, 2750-2756, 2016
99. **Sottmann, J., Homs-Regojo, R., Wragg, D.S., Fjellvåg, H., Margadonna, S., Emerich, H.** *Versatile electrochemical cell for Li/Na-ion batteries and high-throughput setup for combined operando X-ray diffraction and absorption spectroscopy* J. Appl. Cryst., **49**, 1-10, 2016
100. **Storm, M.M., Johnsen, R.E., Norby, P.** *In situ X-ray powder diffraction studies of the synthesis of graphene oxide and formation of reduced graphene oxide* J. Solid State Chemistry, **240**, 49-54, 2016
101. **Storm, M.M., Johnsen, R.E., Younesia, R., Norby, P.** *Capillary based Li–air batteries for in situ synchrotron X-ray powder diffraction studies* J. Mater. Chem. A, **3**, 3113-3119, 2015
102. **Subramanian, V., Ordomsky, V., Legras, B., Cheng, K., Cordier, C., Chernavskii, P., Khodakov, A.** *Design of iron carbon-silica composite catalysts with enhanced catalytic performance in high–temperature Fischer-Tropsch synthesis* Catal. Sci. Technol., **6**, 4953-4961, 2016
103. **Suwarno, S., Solberg, J.K., Krogh, B., Raaen, S., Yartys, V.A.** *High temperature hydrogenation of Ti–V alloys: The effect of cycling and carbon monoxide on the bulk and surface properties* Int. J. Hydrogen Energy, **41б** 3б 1699-1710, 2016
104. **Svitlyk, V., Chernyshov, D., Mozharivsky, Y., Yuan, F., Zaharko, O., Mezouar, M**. *Temperature- and Pressure-Induced Spin Crossover in $Co_{1+x}Cr_{2-x}Se_4$ (x = 0.24): A Diffraction Study* Inorg. Chem., **55**, 1, 338–344, 2016
105. **Szirmai, P., Náfrádi, B., Arakcheeva, A., Szilágyi, E., Gaál, R., Nemes, N.M., Berdat, X., Spina, M., Bernard, L., Jacimovic, J., Magrez, A., Forró, L., Horváth E**. *Cyan titania nanowires: Spectroscopic study of the origin of the self-doping enhanced photocatalytic activity* Catalysis Today, in press, 2016
106. **Thalmann, V., Voegelin, A., Morgenroth, E., Kaegi, R.** *Effect of humic acid on the kinetics of silver nanoparticle sulfidation* Environ. Sci.: Nano, **3**, 203-212, 2016
107. **Tsakoumis, N. E., Johnsen, R. E., Van Beek, W., Ronning, M., Rytterad, E., Holmen, A.** *Capturing metal-support interactions in situ during the reduction of a Re promoted Co/γ - Al_2O_3catalyst* Chem. Commun., **52**, 3239-3242, 2016
108. **Tumanov, N.A., Roedern, E., Lodziana, Z., Nielsen, D.B., Jensen, T.R., Talyzin, A.V., Cerný, R., Chernyshov, D., Dmitriev, V., Palasyuk, T., Filinchuk, Y.** *High-pressure study of $Mn(BH_4)_2$reveals a stable polymorph with high hydrogen density* Chem. Mater., **28**, 1, 274-283, 2016
109. **Valkovskiy, G. A., Altynbaev, E. V., Kuchugura, M. D., Yashina, E.G., Sukhanov, A.S., Dyadkin, V.A., Tsvyashchenko, A.V., Sidorov, V.A., Fomicheva, L.N., Bykova, E., Ovsyannikov, S.V., Chernyshov, D.Yu., Grigoriev, S.V**. *Thermal expansion of monogermanides of 3d-metals* J. Physics: Condensed Matter**, 28**, 37, 2016
110. **Veliks, J., Seifert, H.M., Frantz, D.K., Klosterman, J.K., Tseng, J.Ch., Lindena, A., Siegel, J.S**. *Towards the molecular Borromean link with three unequal rings: double-threaded ruthenium(II) ring-in-ring complexes* Org. Chem. Front., **3**, 667-672, 2016
111. **Vergentev, T., Bronwald, I., Chernyshov, D., Gorfman, S., Ryding, S. H. M., Thompson, P., Cernik, R. J**. *A rapid two-dimensional data collection system for the study of ferroelectric materials under external applied electric fields* J. Appl. Cryst., **49**, 2016
112. **Viani, A., Peréz-Estébanez, M., Pollastri, S., Gualtieri A.F.** *In situ synchrotron powder diffraction study of the setting reaction kinetics of magnesium-potassium phosphate cements* Cement and Concrete Research, **79**, 344-352, 2016

113. **White, J. S., Honda, T., Sibille, R., Gauthier, N., Dmitriev, V., Strässle, Th., Niedermayer, Ch., Kimura, T., Kenzelmann, M.** *Stress-induced magnetic domain selection reveals a conical ground state for the multiferroic phase of Mn_2GeO_4* Phys. Rev. B **94**, 024439-024449, 2016
114. **Yot, P.G., Miele, Ph., Demirci, U.B.** *In situ Synchrotron X-ray Thermodiffraction of Boranes* Crystals**, 6**, 2, 16-28, 2016
115. **Yot, P.G., Yang, K., Guillerm, V., Ragon, F., Dmitriev, V., Parisiades, P., Elkaïm, E., Devic, Th., Horcajada, P., Serre, Ch., Stock, N., Mowat, J.P.S., Wright, P.A., Férey, G., Maurin, G**. *Impact of the Metal Centre and Functionalization on the Mechanical Behaviour of MIL-53 Metal–Organic Frameworks European* J. Inorganic Chemistry, **27**, 4424-4429, 2016
116. **Yot, P.G., Yang, K., Ragon, F., Dmitriev, V., Devic, Th., Horcajada, P., Serre, Ch., Maurin, G.** *Exploration of the mechanical behavior of Metal Organic Frameworks UiO-66(Zr) and MIL-125(Ti) and their NH_2 functionalized version* Dalton Trans., **45**, 4283-4288, 2016
117. **Yuan, R., Claes, N., Verheyen, E., Tuel, A., Bals, S., Breynaert, E., Martensa, J.A., Kirschhock, Ch.E.A.** *Synthesis of an IWW-type germanosilicate zeolite using 5-azonia-spiro[4,4]nonane as a structure directing agent* New J. Chem., **40,** 4319-4324, 2016
118. **Yüzbasi, N.S., Kierzkowska, A.M., Imtiaz, Q., Abdala, P.M., Kurlov, A., Rupp, J.L.M., Mueller, Ch.R.** *ZrO2-Supported Fe2O3 for Chemical-Looping Based Hydrogen Production: Effect of pH on Its Structure and Performance as Probed by X-Ray Absorption Spectroscopy and Electrical Conductivity Measurements* J. Phys. Chem. C, **120**, 34, 18977-18985, 2016
119. **Zacharaki, E., Kalyva, M., Fjellvåg, H., Sjåstad, A. O.** *Burst nucleation by hot injection for size controlled synthesis of ε-cobalt nanoparticles* Chemistry Central J., **10**, 10-21, 2016
120. **Zakharov, B. A., Goryainov, S. V., Boldyreva, E. V.** *Unusual seeding effect in the liquid-assisted high-pressure polymorphism of chlorpropamide* CrystEngComm, **18**, 5423-5428, 2016
121. **Zakharov, B.A., Seryotkin, Y.V., Tumanov, N.A., Paliwoda, D., Hanfland, M., Kurnosov, A.V., Boldyreva, E.V.** *The role of fluids in high-pressure polymorphism of drugs: different behaviour of â-chlorpropamide in different inert gas and liquid media* RSC Adv., **6**, 92629-92637, 2016
122. **Zavorotynska, O., Deledda, S., Hauback, B.C.** *Kinetics studies of the reversible partial decomposition reaction in $Mg(BH_4)_2$* Int. J. Hydrogen Energy, **41**, 23, 9885-9892, 2016
123. **Zhang, Y., Gao, P., Oveisi, E., Lee, Y., Jeangros, Q., Grancini, G., Paek, S., Feng, Y., Nazeeruddin, M.K.** *PbI2-HMPA Complex Pretreatment for Highly Reproducible and Ef-ficient CH3NH3PbI3 Perovskite Solar Cells* J. Am. Chem. Soc., **138**, 43, 14380-14387, 2016
124. **Zhukova, E.S., Mikheykin, A.S., Torgashev, V.I., Bush, A.A., Yuzyuk, Yu.I., Sashin, A.E. , Prokhorov, A.S., Dressel, M., Gorshunov, B.P.** *Crucial influence of crystal site disorder on dynamical spectral response in artificial magnetoplumbites* Solid State Sciences, **62,** 13-21, 2016